REPORT 1159

IMPINGEMENT OF WATER DROPLETS ON WEDGES AND DOUBLE-WEDGE AIRFOILS AT SUPERSONIC SPEEDS [1]

By JOHN S. SERAFINI

SUMMARY

An analytical solution is presented for the equations of motion of water droplets impinging on a wedge in a two-dimensional supersonic flow field with an attached shock wave. The closed-form solution yields analytical expressions for the equation of the droplet trajectory, the local rate of impingement and the impingement velocity at any point on the wedge surface, and the total rate of impingement. The analytical expressions are utilized in the determination of the impingement of water droplets on the forward surfaces of symmetrical double-wedge airfoils in supersonic flow fields with attached shock waves.

For a wedge, the results provide information on the effects of the droplet size, the free-stream Mach number, the semiapex angle, and the pressure altitude. For the double-wedge airfoil, additional calculations provide information on the effect of airfoil thickness ratio, chord length, and angle of attack.

The results for the symmetrical double-wedge airfoil are also correlated in terms of the total collection efficiency as a function of a relative modified inertia parameter. The results are presented for the following ranges of variables: free-stream static temperature, 420° to 460° R; droplet diameter, 2 to 100 microns; free-stream Mach number, 1.1 to 2.0; semiapex angle for the wedge, 1.14° to 7.97°, and corresponding double-wedge-airfoil thickness-to-chord ratio, 0.02 to 0.14; pressure altitude, sea level to 30,000 feet; and chord length, 1 to 20 feet.

INTRODUCTION

The problem of ice prevention on aircraft flying at subsonic speeds up to critical Mach numbers has been a subject of considerable study and research by the NACA. The recent advent of aircraft flying at transonic and supersonic speeds has required an extension of these icing studies. That an icing problem exists in the transonic and supersonic speed range is verified in reference 1, which shows by an analytical investigation with experimental confirmation that diamond or symmetrical double-wedge airfoils are subject to possible icing at flight Mach numbers as high as 1.4. A similar result is expected for other airfoil shapes being considered for use at transonic and supersonic flight speeds.

In conducting research on the problem of ice prevention on aircraft and missiles, regardless of the magnitude of the flight speed, it is essential that the impingement of cloud droplets on airfoils and other aerodynamic bodies be determined either by theoretical calculations or experiment. The impingement variables that must be determined are the total water catch, the extent of impingement, and the rate of impingement per unit area of body surface. These variables can be determined analytically from calculations of the cloud-droplet trajectories obtained for the various aerodynamic bodies. Investigators have reported the results of studies of cloud-droplet trajectories about right-circular cylinders (refs. 2 to 5) and about airfoils (refs. 6 to 9) immersed in an incompressible fluid. An evaluation of the effect of compressibility on the droplet trajectories about cylinders and airfoils up to the critical flight Mach number is presented in reference 10.

At present, little information exists on the impingement of droplets on aerodynamic bodies in a supersonic air stream. The concentration of past effort on problems of impingement on airfoils at subsonic flight speeds and the present lack of convenient and rapid means for obtaining the rotational flow fields about airfoils at supersonic speeds are possible explanations for the scarcity of trajectory calculations for the supersonic region. An initial contribution to the solution of the over-all problem of impingement of water droplets on aerodynamic bodies at supersonic speeds is given in reference 11, which presents an analysis of the water-interception characteristics of a wedge in a supersonic flow field.

The present report extends the analysis of reference 11 and further presents an extensive study of the impingement of water droplets on two-dimensional wedges and double-wedge airfoils for supersonic flight speeds that result in attached shock waves and constant velocity fields behind the shock waves. For the wedge angles and double-wedge-airfoil thickness ratios considered herein, the shock-wave-attachment Mach number varies from a value slightly greater than 1 to about 1.4. The method employed is based on an analytical solution of the equations of motion by means of a closed-form integration. The closed-form solution yields analytical expressions for the equation of the trajectories, the local impingement efficiencies, the velocity at any point on the trajectories, and the total rate of impingement. This solution is made possible by the use of an empirical relation for the drag coefficients for spheres that gives a good approximation of the experimental drag coefficients.

The results of calculations for the rate, the extent, and the distribution of impingement of water droplets on wedges and symmetrical double-wedge airfoils are presented herein.

[1] Supersedes NACA TN 2971, "Impingement of Water Droplets on Wedges and Diamond Airfoils at Supersonic Speeds," by John S. Serafini, 1953.

The ranges of variables included for the wedge are: free-stream static temperature, 420°, 440°, and 460° R; droplet diameter, 2 to 100 microns; free-stream Mach number, 1.1 to 2.0; tangent of the semiapex angle, 0.02 to 0.14; and pressure altitude, sea level, 15,000, and 30,000 feet. The ranges of variables for the double-wedge airfoil are the same as those for the wedge, and the additional variables for the symmetrical double-wedge airfoil range from 0.02 to 0.14 for the thickness ratio and from 1 to 20 feet for the chord length.

The work reported herein was performed at the NACA Lewis laboratory in the spring and summer of 1952.

ANALYSIS

STATEMENT OF PROBLEM

The solution of the problem of impingement of water droplets on a two-dimensional wedge at supersonic speeds with an attached shock wave is not as difficult as that for the impingement on various airfoils at low subsonic speeds. For the wedge at supersonic speeds with an attached shock wave, the air velocity everywhere ahead of the shock wave is constant and equal to the free-stream air velocity V_1 (fig. 1). The air velocity behind the shock wave V_2 is also everywhere constant and parallel to the wedge surface. All the droplets have the same initial velocity (that of the free-stream air velocity), and their trajectories are exactly coincident with the air streamlines upstream of the shock wave. All water droplets of a given size are subjected to identical air-velocity fields, which in turn produce identical force systems downstream of the shock wave, irrespective of the point along the shock wave where the droplets cross the wave. It follows, therefore, that, for droplets of a given size, all the trajectories in a given problem are identical with respect to the point where the droplet crosses the shock wave.

By adopting a frame of reference that moves at the constant velocity of the air V_2 downstream of the shock wave, the problem of the droplet motion is reduced to the still-air problem, defined as the determination of the motion of a droplet that, having an initial velocity, is projected into quiescent air. Hence, relative to the moving frame of reference, the initial velocity of the droplet upon crossing the shock wave is equal to the vectorial difference of the free-stream air velocity V_1 and the air velocity V_2 downstream of the shock wave. Adoption of the frame of reference moving with a constant velocity reduces the problem from the solution of two simultaneous nonlinear second-order differential equations in the fixed coordinate system to the solution of a single nonlinear second-order differential equation in the moving coordinate system. At any given instant, the droplet displacement relative to the point of intersection with the shock wave in the fixed frame of reference is obtained by adding vectorially the droplet displacement within the moving frame of reference to the displacement of the moving frame of reference for the same increment of time.

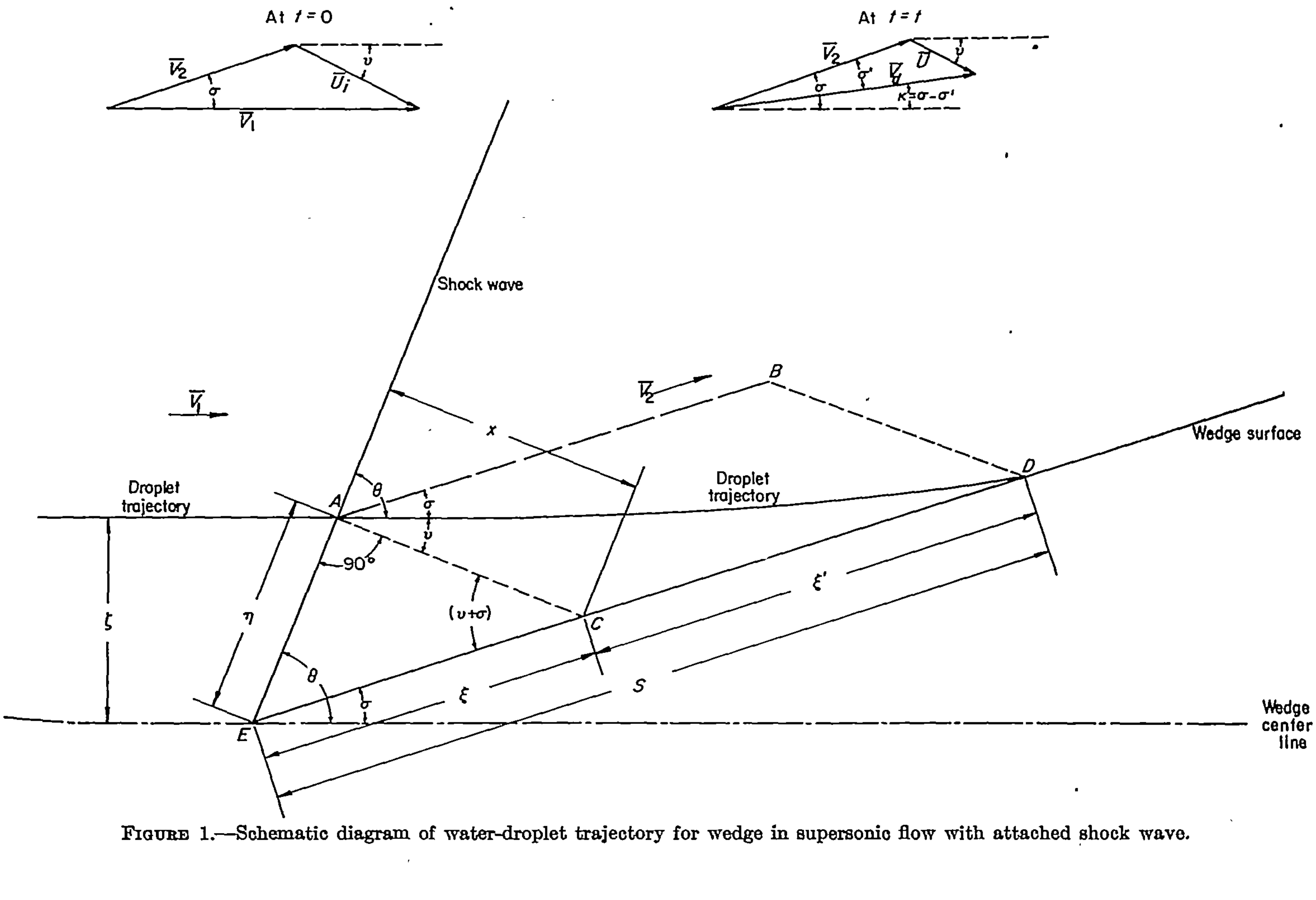

FIGURE 1.—Schematic diagram of water-droplet trajectory for wedge in supersonic flow with attached shock wave.

This general method was used in reference 11, where the one second-order differential equation representing the droplet motion relative to the air velocity behind the shock wave was integrated graphically. However, it is possible to obtain a completely analytical solution by means of a closed-form integration without resorting to the use of numerical integrations or analog computing equipment, if an empirical relation is assumed for the drag coefficient as a function of the Reynolds number of the droplet relative to the air. It will be shown that this closed-form integration of the still-air problem when applied to the wedge in supersonic flow with attached shock wave yields the equations for the trajectories of the water droplets and the droplet velocities at any point on the trajectories and makes available relations for the rates of total water impingement and the local rates of water impingement along the wedge surface. Furthermore, it is shown that these equations can also be readily applied to the determination of the droplet impingement on a double-wedge airfoil in supersonic flow with attached shock wave.

Three of the usual assumptions made in the previous investigations on impingement at subsonic speeds and also required for this investigation are (1) the water droplets are always spherical and do not change in size, (2) the force of gravity on the droplet may be neglected in comparison with the drag forces, and (3) the drag of the air on the droplet is that of a viscous incompressible fluid. Here it is additionally assumed that (4) the two-dimensional supersonic flow field about the wedge is frictionless except within the infinitesimally thin attached shock wave, (5) no condensation shock occurs and no change in phase occurs as the water droplets traverse the oblique shock wave, and (6) the unbalance of the forces on the water droplet from the instant it enters the shock wave until it emerges from the shock wave can be neglected in the calculation of the trajectories.

EQUATION OF DROPLET MOTION IN MOVING REFERENCE FRAME

The velocity of the droplet in the moving frame of reference is

$$U=|\overline{V}_d-\overline{V}_2| \tag{1}$$

where $\overline{V}_d$ is the droplet velocity with respect to the fixed frame of reference, and $\overline{V}_2$ is the air velocity downstream of the attached shock wave also with respect to the fixed frame of reference (fig. 1). In the frame of reference moving with the velocity $\overline{V}_2$, the statement of Newton's law of motion for the water droplet becomes

$$D=-C_D\frac{1}{2}\rho_2\pi a^2U^2=\frac{4}{3}\pi a^3\rho_w\frac{dU}{dt} \tag{2}$$

from which

$$\frac{dU}{dt}=-\frac{3}{8}\frac{\rho_2}{\rho_w}\frac{U^2}{a}C_D \tag{3}$$

(A complete list of symbols is given in appendix A.)

Equation (3) is the differential equation of motion of a droplet projected with an initial velocity into a region of quiescent air (the so-called still-air problem). The shock wave is considered to be a surface of discontinuity from which the droplets emerge with a velocity V_1. In this case the initial velocity of the droplet is

$$U_i=|\overline{V}_1-\overline{V}_2| \tag{4}$$

which is the magnitude of the vector difference of the air-velocity vectors upstream and downstream of the attached shock wave. As can be shown from consideration of the continuity equation and the equation for conservation of momentum across the oblique shock wave, the velocity vector $\overline{U}_i$ is normal to the shock wave. At any subsequent instant of time, the relative droplet velocity vector $\overline{U}$ retains the same angular orientation to the shock wave and changes only in magnitude.

In reference 11 the solution of equation (3) is obtained by numerical integration. The result obtained in this manner makes it necessary to use a graphical procedure in determining the trajectories and the local rates of impingement. However, an analytical solution of equation (2), which eliminates the graphical procedure, can be obtained if the experimental values of the drag coefficient C_D are expressed in a function involving the Reynolds number Re_r. The relation is

$$C_D=\frac{24}{Re_r}(1+\epsilon Re_r^{m}) \tag{5}$$

where ϵ and m are the empirical constants. This empirical relation is a valid approximation in the range of Reynolds numbers to which cloud droplets are subjected in trajectory calculations. Substitution of the expression for C_D (eq. (5)) in equation (3) results in the expression

$$\frac{dU}{dt}=\frac{d^2x}{dt^2}=-\frac{9}{2}\frac{\mu_2}{\rho_w}\frac{U}{a^2}\left[1+\epsilon\left(\frac{2\rho_2Ua}{\mu_2}\right)^m\right] \tag{6}$$

where the local relative Reynolds number $Re_r=2\rho_2Ua/\mu_2$. The displacement of the water droplet in the moving frame of reference x is measured from the air streamline that intersects the shock wave at the point where the water droplet enters the air-flow field downstream of the shock wave. The closed-form integration of the differential equation (6) is presented in appendix B. The use of 2/3 for the exponent m and 0.158 for the value of the empirical constant ϵ in equation (5) yields an empirical curve for the drag coefficient as a function of the local Reynolds numbers that approximates very well the variation of the experimental values of the drag coefficient in the range of Reynolds numbers from 0.5 to 500. The value of 2/3 for the exponent m also facilitates the closed-form integration of the differential equation of motion. In figure 2 a graph of the empirical relation is presented, along with the drag-coefficient data of references 4 and 12.

The results of the integration are given by the following equations:

$$x=\frac{a}{3}\epsilon^{-3/2}\frac{\rho_w}{\rho_2}\left[Re_{r,i}^{1/3}\epsilon^{1/2}+\tan^{-1}(Re_{r,i}^{-1/3}\epsilon^{-1/2})-\frac{1}{\sqrt{(Re_{r,i}^{-2/3}\epsilon^{-1}+1)e^{\tau}-1}}-\tan^{-1}\sqrt{(Re_{r,i}^{-2/3}\epsilon^{-1}+1)e^{\tau}-1}\right] \tag{7}$$

$$U=\frac{U_t}{Re_{r,t}\epsilon^{3/2}}\left[(Re_{r,t}^{-2/3}\epsilon^{-1}+1)\,e^{\tau}-1\right]^{-3/2} \tag{8}$$

and

$$x_m=\frac{a}{3}\,\epsilon^{-3/2}\,\frac{\rho_w}{\rho_2}\left(Re_{r,t}^{1/3}\epsilon^{1/2}-\frac{\pi}{2}+\varphi\right) \tag{9}$$

where

$$\varphi=\tan^{-1}(Re_{r,t}^{-1/3}\epsilon^{-1/2});\qquad 0\leqq\varphi\leqq\frac{\pi}{2}$$

The intermediate steps of integration are given in appendix B.

Equations (7) and (8) give, respectively, the displacement and the velocity of the droplet at any instant in the moving frame of reference. The displacement of the droplet with respect to the point where it crosses the shock wave can be obtained by a vectorial addition of the displacement x and the displacement of the moving reference frame in the corresponding time interval. The droplet velocity $\overline{V}_d$ relative to the fixed frame of reference must also be obtained by the vectorial addition of $\overline{U}$ (eq. (8)) and $\overline{V}_2$. Equation (9) gives the maximum value of x obtained as the time of travel in the air-flow field downstream of the shock wave approaches infinity. The significance of this quantity will be discussed in subsequent sections.

RELATIONS REQUIRED FOR APPLICATION OF CLOSED-FORM SOLUTION TO OBTAIN DROPLET MOTION AND IMPINGEMENT IN FIXED REFERENCE FRAME

Impingement on wedges.—For a problem of given aerodynamic conditions, the trajectories of all the water droplets of a given size are identical when the points where the droplet trajectories intersect the shock wave are superimposed. This unique characteristic of the water-droplet trajectories about a wedge in supersonic flow with an attached oblique shock wave is the result of two constant velocity fields, one upstream and one downstream of the shock wave. Therefore, only one set of equations for a single trajectory is necessary to calculate the impingement parameters for a specified problem, including a given droplet size. The values of the initial relative velocity U_t, the initial Reynolds number $Re_{r,t}$, and the density ratio ρ_w/ρ_2 are needed for substitution in the closed-form solution of the equations of droplet motion. These values can be obtained from information available in reference 13 and from the use of simple algebraic and trigonometric relations for given values of the free-stream static temperature t_1, the droplet diameter d, the free-stream Mach number M_1, the angle of surface inclination to the free-stream direction σ, and the free-stream static pressure p_1. These relations result in the following expressions for the initial relative velocity and the initial relative Reynolds number:

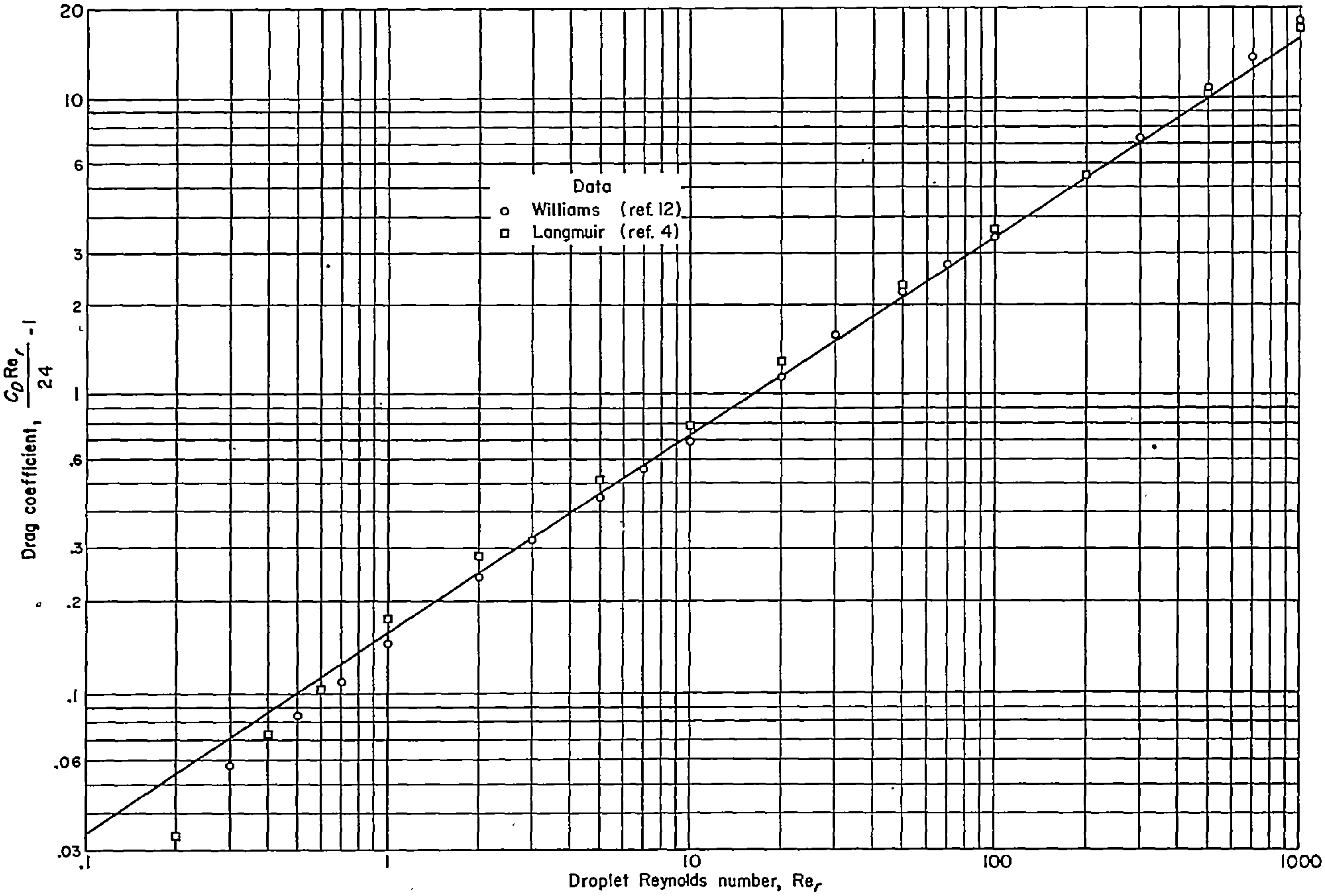

FIGURE 2.—Comparison of empirical relation for drag coefficient as function of droplet Reynolds number with experimental values.

$$\frac{C_D Re_r}{24}=1+0.158Re_r^{2/3}$$

$$U_t=|\overline{U}_t|=V_1\sqrt{1+\Omega^2-2\Omega\cos\sigma}=V_1\omega \tag{10}$$

and

$$Re_{r,t}=2\sqrt{\frac{\gamma}{gR}}\frac{ap_1}{\mu_2 t_1^{1/2}}M_1\omega\frac{\rho_2}{\rho_1} \tag{11}$$

A convenient form of the solution for the impingement on a wedge or the front half of a double-wedge airfoil is obtained if S is defined as the distance to the point of impingement measured from the leading edge for a water droplet that enters the flow field behind the shock wave at a distance ζ above the leading edge (fig. 1). The unique relation between S and ζ in a given problem for droplets of the same size is quite readily determined by considering the displacement of the water droplets as the vectorial sum of the displacement of the water droplet relative to the moving frame of reference and the displacement of the moving reference frame relative to a fixed frame of reference (referred to wedge). Since the moving reference frame has a velocity equal to the air velocity V_2, which is constant in magnitude and parallel to the wedge surface, only the droplet travel in the moving reference frame includes the component of droplet travel representing the approach of the water droplet to the wedge surface. For a water droplet starting from point A and impinging on the wedge surface at point D (fig. 1), the displacement of the moving reference frame ($=V_2t$, where t is zero at point A) is given by the displacement vector $\overline{AB}$ equal to $\overline{CD}$, and the droplet motion in the moving frame of reference is given by the displacement vector $\overline{BD}$ equal to $\overline{AC}$. Therefore, relative to the starting point at A (fig. 1), the displacement of the water droplet to the point of impingement at D is obviously equal to $\overline{AB}+\overline{BD}$ or to $\overline{AC}+\overline{CD}$. From figure 1, the displacement of the water droplet at the point of impingement D, measured from the leading edge at E, is given by adding the vector $\overline{EA}$ to the displacement vector from the starting point A; and the displacement of the droplet at D referred to the leading edge is

$$S=|\overline{ED}|=|\overline{EA}+\overline{AC}+\overline{CD}|=|\overline{EC}+\overline{CD}|=|\overline{EC}|+|\overline{CD}|=\xi+\xi' \tag{12}$$

where ξ is the magnitude of the displacement vector $\overline{EC}$, and ξ' ($=V_2t$) is the magnitude of the displacement vector $\overline{CD}$ (the displacement of the moving frame of reference).

The values of ζ and ξ are obtained in terms of x, the distance of travel in the moving reference frame, from simple trigonometric identities involving the various angles shown in figure 1:

$$\zeta=x\sin\theta\tan(\nu+\sigma) \tag{13}$$

where x is given by equation (7); ν by

$$\nu=\sin^{-1}\left[(\sin\sigma)\frac{\Omega}{\omega}\right] \tag{13a}$$

and

$$\xi=x\sec(\nu+\sigma) \tag{14}$$

Substitution of equation (14) into equation (12) for the surface distance to the point of impingement yields the following equation:

$$S=x\sec(\nu+\sigma)+V_2\frac{\rho_w a^2}{3\mu_2}\tau \tag{15}$$

Since x is a function of τ in equations (13) and (15), the expressions for ζ and S, respectively, are functions of τ. However, since τ cannot be eliminated from equations (13) and (15), S cannot be obtained explicitly as a function of ζ. Nevertheless, the curves of ζ, the initial displacement of the water-droplet trajectory from the leading edge normal to the free-stream direction, against S, the distance to the point of impingement of the stated water-droplet trajectory, can be obtained by substitution of the same set of values for τ in the expressions for ζ and S.

An analytical expression for the local impingement efficiency can be obtained from the preceding expressions for ζ and S. The local impingement efficiency β is defined by the expression

$$\beta=\lim_{\Delta S\to 0}\left(\frac{\Delta\zeta}{\Delta S}\right)=\frac{d\zeta}{dS}=\frac{\frac{d\zeta}{d\tau}}{\frac{dS}{d\tau}} \tag{16}$$

where $\Delta\zeta$ is the difference in the initial displacements of two water droplets having very nearly equal initial displacements, and ΔS is the small increment of wedge surface between the points of impingement of the two water droplets. Differentiating ζ and S with respect to τ and performing the division indicated by equation (16) yield the following expression for β:

$$\beta=\frac{1}{\frac{n_2}{n_1}+\frac{n_3}{n_1}\frac{6\epsilon^{3/2}}{a}\frac{\rho_2}{\rho_w}[(Re_{r,t}{}^{-2/3}\epsilon^{-1}+1)e^{\tau}-1]^{3/2}} \tag{17}$$

where

$$n_1=\sin\theta\tan(\nu+\sigma) \tag{18a}$$

$$n_2=\sec(\nu+\sigma) \tag{18b}$$

$$n_3=V_2\frac{\rho_w a^2}{3\mu_2}=V_2\frac{t}{\tau} \tag{18c}$$

Since β and S both are functions of τ, the local impingement efficiency β at any point on the wedge surface is determined by using the same value of τ in equations (17) and (15). The value of β that exists as the point of impingement of the water droplet on the wedge surface approaches the leading edge as a limit ($S\to 0$) is given by the following:

$$\beta_0=\lim_{S\to 0}(\beta)=\frac{1}{\frac{n_2}{n_1}+\frac{n_3}{n_1}\frac{3}{a^2}\frac{\mu_2}{\rho_w}\frac{1}{U_t}}=\sin\sigma \tag{19}$$

The magnitude and direction of the droplet velocity at the point of impingement $V_{d,im}$ (relative to the fixed frame of reference) can also be easily obtained at any point on the wedge surface as

$$V_{d,im}=V_1\sqrt{\Omega^2+\omega^2\left(\frac{U_{im}}{U_t}\right)^2+2\Omega\omega\frac{U_{im}}{U_t}\cos(\nu+\sigma)} \tag{20}$$

$$\kappa_{im}=\sigma-\sigma'_{im}=\sigma-\sin^{-1}\left[\frac{U_{im}}{V_{d,im}}\sin(\nu+\sigma)\right] \tag{21}$$

where κ is the angle between the free-stream velocity vector

V_1 and the droplet-velocity vector $\overline{V}_d$, and σ' is the angle between the droplet-velocity vector $\overline{V}_d$ and the air-velocity vector $\overline{V}_2$. In equations (20) and (21) for a given trajectory, V_1, Ω, ω, U_t, ν, and σ are constants. Therefore, for a given trajectory, $V_{d,tm}$ and κ_{tm} are functions only of U (eq. (8)), which is in turn a function of τ, the dimensionless time variable.

Impingement on symmetrical double-wedge airfoils.—The impingement on a double-wedge airfoil may be obtained from the solution to the problem of impingement on a wedge as presented heretofore. In this report, the double-wedge airfoil considered is symmetrical, the maximum thickness occurring at 50 percent of chord (fig. 3). At zero angle of attack, the impingement on a double-wedge airfoil will be limited to the region from the leading edge to the shoulder at 50 percent of chord. The solution for impingement on a wedge surface having a given semiapex angle σ (the angle of inclination of either wedge surface to the free-stream direction) can also be used as the solution for a double-wedge airfoil where the thickness ratio is equal to tan σ, the tangent of the semiapex angle, and where the droplet size and other parameters of the problem are the same as for the wedge. Therefore, the values of the local impingement efficiencies β and β_0 at any given point on the surface will be identical for both the wedge and the double-wedge airfoil at zero angle of attack under the aforementioned similarity of conditions.

The solution for the impingement on the double-wedge airfoil at angle of attack can also be obtained from the solution for impingement on a wedge as for the case of the double-wedge airfoil at zero angle of attack. When the symmetrical double-wedge airfoil is at angle of attack α, the angle of inclination of its forward upper surface to the free-stream direction is equal to $\sigma-\alpha$ and that of the forward lower surface is equal to $\sigma+\alpha$. Therefore, the solution to the impingement on the upper and lower surfaces of the double-wedge airfoil is obtained from the solutions for impingement on wedges having the redefined semiapex angles of $\sigma-\alpha$ and $\sigma+\alpha$, respectively, where the droplet size and other parameters of the problem are kept the same. For the double-wedge airfoils at angles of attack having tangents equal to or greater than the thickness ratio, the water droplets will not impinge on the upper surface. At angles of attack having tangents greater than the thickness ratio, some water droplets may impinge on the lower surface beyond 50 percent of chord. These three conditions are illustrated schematically in figure 3. For $\alpha<\tan^{-1}(T/c)$, the impingement occurs on surfaces AC and AB; for $\alpha=\tan^{-1}(T/c)$, impingement occurs only on surface AC; for $\alpha>\tan^{-1}(T/c)$, impingement occurs on lower surface AC and may occur on lower surface CD. However, the condition where $\alpha>\tan^{-1}(T/c)$ is not considered herein, since the solution presented in this report is not valid for the determination

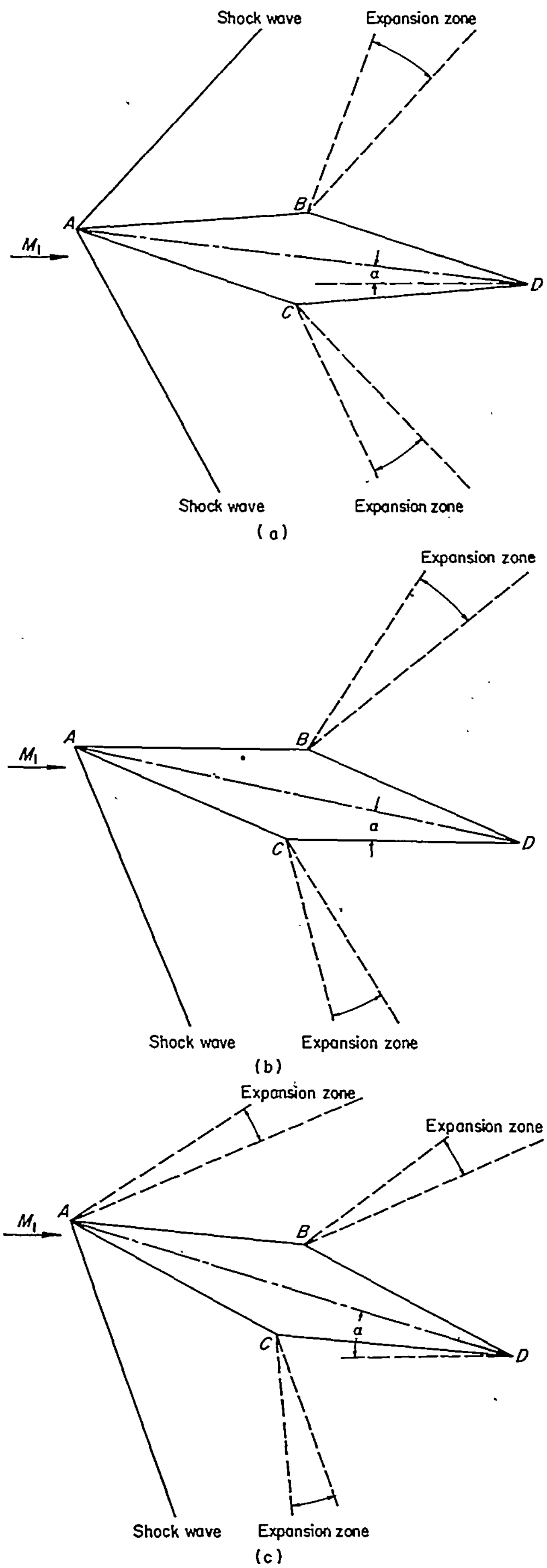

(a) Angle of attack $\alpha<\tan^{-1}(T/c)$.
(b) Angle of attack $\alpha=\tan^{-1}(T/c)$.
(c) Angle of attack $\alpha>\tan^{-1}(T/c)$.

FIGURE 3.—Schematic diagram of symmetrical double-wedge airfoil at angle of attack in supersonic flow with attached shock wave.

of trajectories of droplets impinging on the surface beyond the shoulder or 50 percent of chord of the double-wedge airfoil (surfaces BD or CD), where a portion of the trajectories is within the expansion zone emanating from the shoulder.

RESULTS AND DISCUSSION

From the equations presented in the previous section and in appendix B, the impingement of water droplets on a wedge in a supersonic flow field with an attached shock wave can be calculated over a range of free-stream conditions, wedge angles, and droplet sizes. As has been indicated previously, the impingement characteristics of a double-wedge airfoil (at zero angle of attack and also for small values of angle of attack) can readily be determined from the impingement on wedges for similar conditions. The results for the wedge and the double-wedge airfoil are presented and discussed separately. A comparison of the total collection efficiency and the water impingement rate at zero angle of attack for a double-wedge airfoil with those for an NACA 0006–64 airfoil is presented in appendix C.

WEDGE

Local impingement efficiency.—The rate of water impingement on a local area of wedge or airfoil surface is proportional to a dimensionless term β, the local impingement efficiency. The local rate of water impingement in pounds per hour per square foot is

$$W_\beta = 0.3296 V_1 w \beta$$

where β is defined in equation (16). The local impingement efficiency, when given as a function of the surface distance of the wedge, allows the determination of the local rate of impingement of water droplets at any point on the surface, the total impingement of water droplets on the entire surface or any given portion of the surface, and the extent of impingement on the surface. The local impingement efficiency β is related to a point at a given distance S on the wedge surface in equations (15), (17), and (19) by the dimensionless time variable τ, which is common to all three expressions. The variation of β with S is presented in figure 4 for an extensive range of free-stream conditions, semiapex angles, and droplet sizes. The value of β at the leading edge ($S \rightarrow 0$) is the sine of the semiapex angle ($\sin \sigma$); and as S increases, the value of β decreases rapidly and approaches the value of zero asymptotically as S approaches infinity. However, it is to be noted that negligibly small values of β ($\beta \approx 1$ percent of β_0 for the wedge) are attained at large but finite values of S.

The curves of β as a function of S presented in figure 4 are those of an idealized situation. The assumed two-dimensional supersonic flow field about the wedge does not account for a stagnation point that must exist at the leading edge of the wedge, regardless of the sharpness of the leading edge. In addition, the leading edges of wedges and double-wedge airfoils might be considered to be somewhat rounded when subjected to considerable magnification. Therefore, it is reasonable to assume that very near the leading edge ($S \rightarrow 0$) the value of β would actually be greater than the calculated value of β at the given distance S. However, this should have a negligible effect on the rest of the β curve and also on the total impingement on the wedge, since the effect of a stagnation point would be limited to a very small region about the leading edge.

For S approaching very large values, the calculated values of β probably differ somewhat from actual values obtained in flight, because the analytical solution of the present report does not consider the existence of the boundary layer on the wedge surface. Since the boundary-layer thickness increases with the surface distance along the wedge, droplets that im-

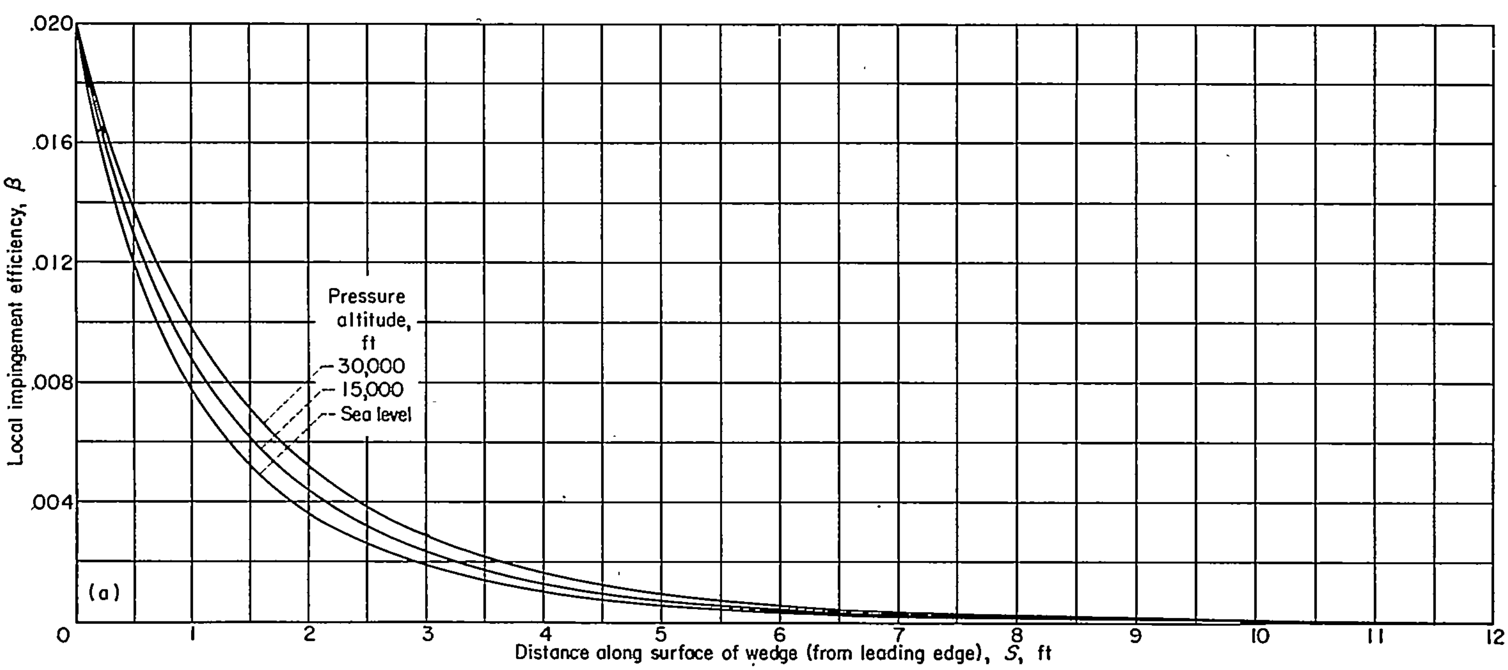

(a) Effect of pressure altitude. Droplet diameter, 20 microns; free-stream Mach number, 1.4; tangent of semiapex angle, 0.02.

FIGURE 4.—Local impingement efficiency on wedge as function of distance along surface. Free-stream static temperature, 440° R.

pinge at large distances from the leading edge actually would have traveled through the boundary layer for some non-negligible interval of time. However, only a very small fraction of the total water droplets of a given size impinge under this condition, and for large values of S the values of β are negligibly small. For example (fig. 4 (a)), such would be the case for values of S greater than 8 or 9 feet, where $\beta<0.0002$ as compared with $\beta_0=0.020$.

A preliminary survey disclosed a negligible effect of the free-stream static temperature on the local impingement efficiency as a function of the surface distance along the wedge (β against S). Values of β and corresponding values of S were calculated for free-stream static temperatures of 420°, 440°, and 460° R, droplet diameter of 20 microns, free-stream Mach number of 1.3, tangent of the semiapex angle of 0.06, and pressure altitude of 15,000 feet. The values of β for the free-stream static temperatures of 420° and 460° R are within 1 percent of the values of β at 440° R. Since these calculations show that curves of β against S for the three values of free-stream static temperature form practically a single curve when plotted to the usual scales, no figure is presented to illustrate the effect of free-stream static temperature on impingement. Furthermore, the results included herein, which are calculated for a free-stream static temperature of 440° R, may be used in the range of temperature from 420° to 460° R or possibly an even greater range.

The effect of the free-stream static pressure on the local impingement efficiency as a function of the surface distance along the wedge is presented in figure 4 (a) for pressure altitudes of sea level, 15,000, and 30,000 feet. Increasing the pressure altitude (decreasing the free-stream static pressure) increases the values of β at any distance S. For example, at $S=1.5$ at sea level, β is 0.0052; and at 30,000 feet, β is 0.0071. Since β_0 (the value of β at $S=0$) is equal to $\sin\sigma$, where σ is the semiapex angle, the curves for the three pressure altitudes have the same maximum value of β. Also, for the various pressure altitudes, the extent of impingement along the wedge surface is essentially the same.

The effect of the semiapex angle σ of the wedge on the local impingement efficiency as a function of the surface distance along the wedge is presented in figure 4 (b) for values of $\tan\sigma$ from 0.02 to 0.10. Since the values of β_0 are equal to $\sin\sigma$, increasing the semiapex angle of the wedge results in an increase of β_0. The surface extent of perceptible impingement (as characterized by $\beta\approx 0.01\beta_0$) does not vary as the wedge thickness is increased.

The effect of free-stream Mach number on the β curve is presented in figure 4 (c) for free-stream Mach numbers of 1.2, 1.3, 1.4, 1.5, and 2.0. For the wedge semiapex angle presented in the figure ($\tan\sigma=0.04$), the value of $M_1=1.2$ is close to the shock-wave-attachment Mach number. The shock-wave-attachment Mach number is a function of the wedge semiapex angle and is defined as that Mach number below which the shock wave is detached from the wedge. An increase in the free-stream Mach number M_1 results in an increased surface extent of perceptible impingement and also in an increased value of β at any given distance S (except

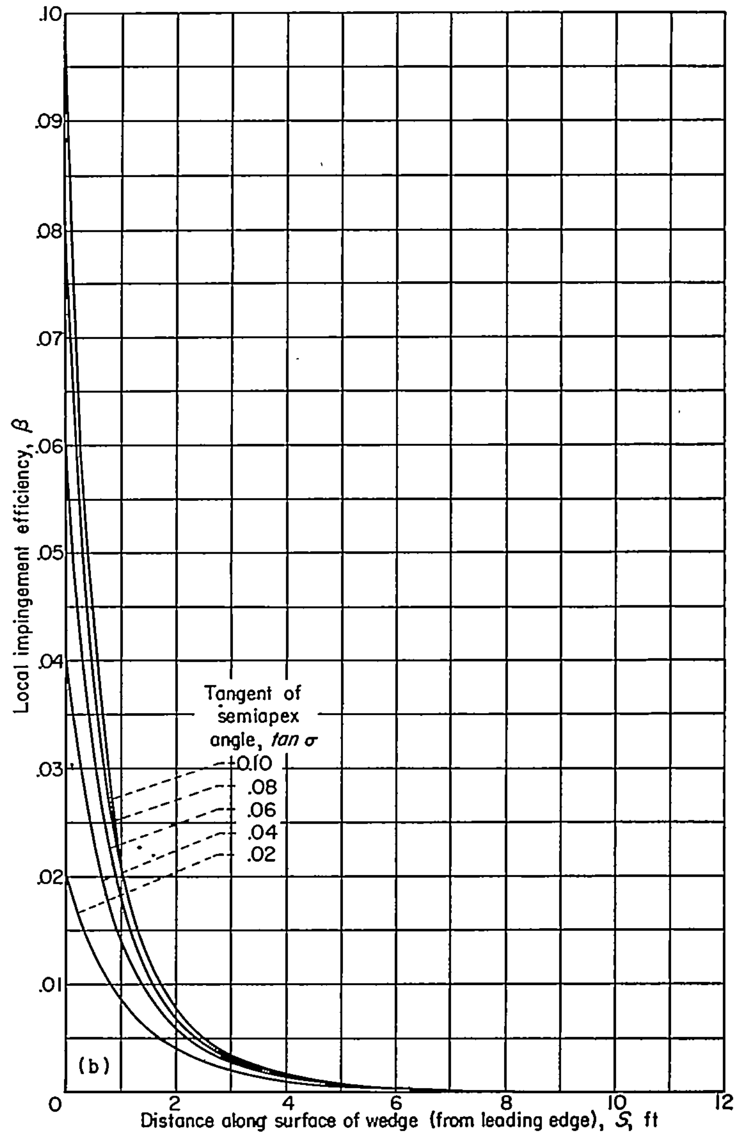

(b) Effect of wedge semiapex angle. Droplet diameter, 20 microns; free-stream Mach number, 1.3; pressure altitude, 15,000 feet.

Figure 4.—Continued. Local impingement efficiency on wedge as function of distance along surface. Free-stream static temperature, 440° R.

at $S=0$, where $\beta\equiv\beta_0\equiv\sin\sigma$ and at $S\rightarrow\infty$, where $\beta\rightarrow 0$). This increase in the surface extent of perceptible impingement is shown in figure 4 (c), in which, for free-stream Mach numbers of 1.2, 1.3, 1.4, 1.5, and 2.0, the surface extents of perceptible impingement on the wedge (where $\beta\approx 0.01\beta_0$) are 5.35, 6.05, 6.65, 7.20, and 9.4 feet, respectively.

The effect of the droplet size on β is presented in figure 4 (d) for droplet diameters of 10, 20, 30, 40, 50, and 100 microns. The surface extent of impingement and the values of β at any given distance S are considerably increased as the droplet size is increased. For example, for the semiapex angle presented in the figure ($\tan\sigma=0.06$), at $S=3$ feet the values of β are 0.0000, 0.0033, 0.0106, 0.0182, 0.0244, and 0.0417 for values of droplet diameter of 10, 20, 30, 40, 50, and 100 microns, respectively. The surface extent of perceptible impingement has values of 1.5, 5.7, 11.2, 18.1, and

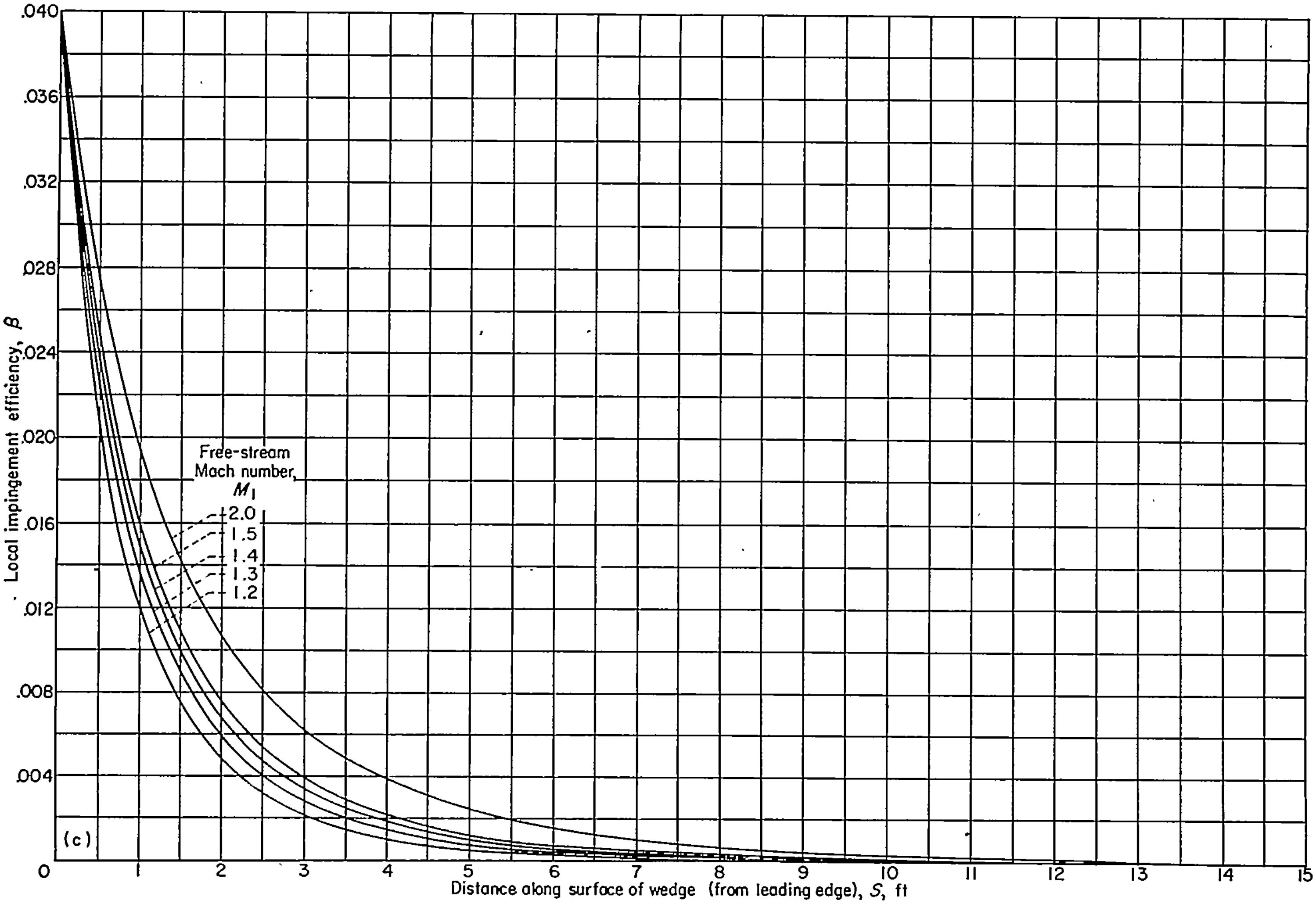

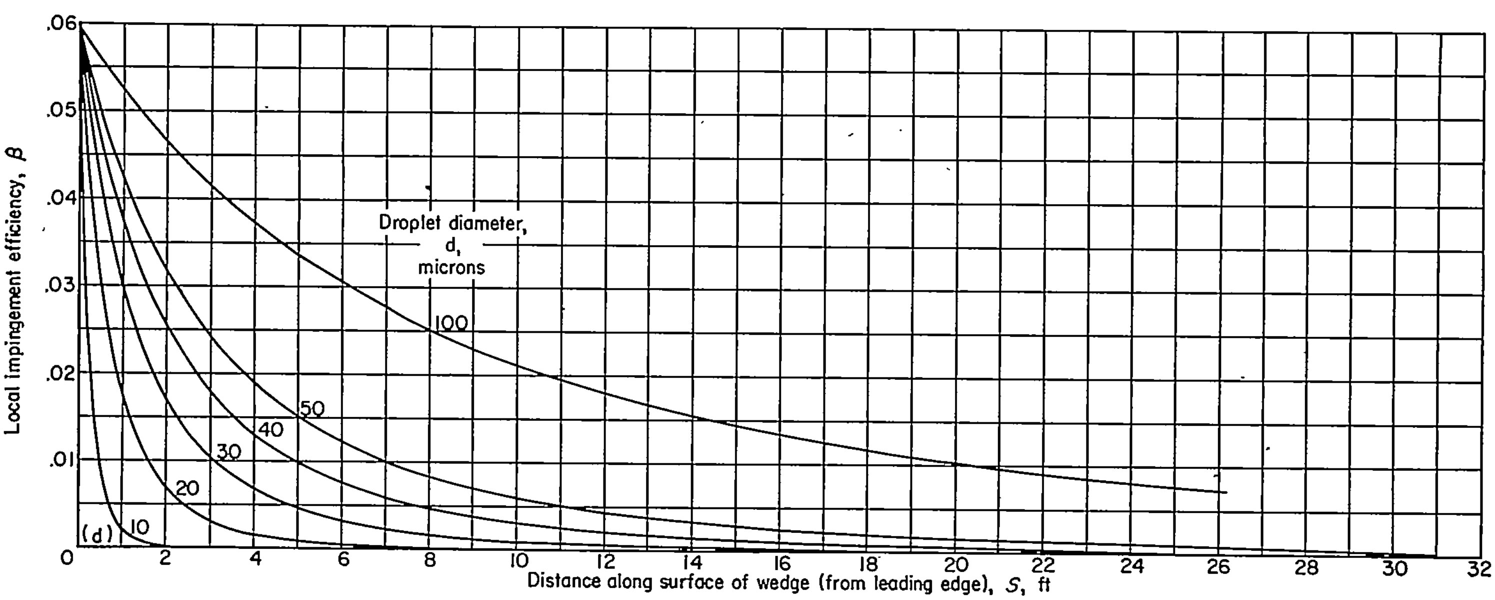

(c) Effect of free-stream Mach number. Droplet diameter, 20 microns; tangent of semiapex angle, 0.04; pressure altitude, 15,000 feet.
(d) Effect of droplet size. Free-stream Mach number, 1.3; tangent of semiapex angle, 0.06; pressure altitude, 15,000 feet.

FIGURE 4.—Concluded. Local impingement efficiency on wedge as function of distance along surface. Free-stream static temperature, 440° R.

28.0 feet for droplet diameters of 10, 20, 30, 40, and 50 microns, respectively. As shown by the preceding discussion and also by a comparison of the values of β as a function of S (fig. 4), varying the droplet diameter from 20 to 30 microns or from 30 to 40 microns is of the same order of magnitude in its effect on the β against S curve as varying the pressure altitude from sea level to 30,000 feet or varying the free-stream Mach number from 1.2 to 1.5.

Total impingement.—The effects of the free-stream Mach number, the semiapex angle of the wedge, the pressure altitude, and the droplet size on the total impingement on a wedge surface of infinite extent are given in figure 5. The total impingement is represented by ζ_m, which is the ζ of the droplet having its trajectory tangent to the wedge surface (theoretically the tangent trajectory touches the wedge surface at a point $S \rightarrow \infty$). This ζ_m can be obtained from the integration

$$\zeta_m = \int_0^\infty \beta dS$$

or more directly from equation (13) of the analytical solution, as

$$\zeta_m = x_m \sin \theta \tan (\nu + \sigma)$$

where x_m is given by equation (9) and is also defined in appendix A. The value for x_m is obtained from the expression for x (eq. (7)) by allowing $\tau \rightarrow \infty$. Since the droplet that enters the flow field downstream of the shock wave at a distance ζ equal to ζ_m (fig. 1) theoretically impinges on the wedge surface only as the surface distance S approaches infinity, only droplets having values of ζ equal to or less than ζ_m will impinge on the wedge surface of infinite extent. The rate of total water catch on one wedge surface in terms of ζ_m is given as

$$W_m = 0.3296 \zeta_m V_1 w$$

where W_m is expressed in pounds per hour per foot of span, V_1 in miles per hour, and w in grams per cubic meter. Therefore, ζ_m is directly proportional to the rate of total water catch on the entire wedge surface and is the rate of total water catch on one wedge surface per unit of span, free-stream velocity, and liquid-water content (in appropriate units).

The variation of ζ_m with the tangent of the wedge semiapex angle $\tan \sigma$ is shown in figure 5 (a) for free-stream Mach numbers of 1.2, 1.3, 1.4, and 2.0. As expected from the curves of β as a function of S, the value of ζ_m increases as $\tan \sigma$ increases. However, the rate of increase in ζ_m with respect to $\tan \sigma$ decreases with an increase in $\tan \sigma$. As can be seen from figure 5 (a), increasing the free-stream Mach number increases the value of ζ_m for a constant value of $\tan \sigma$.

The variation of ζ_m with pressure altitude is presented in figure 5 (b) for two Mach numbers. In the range of pressure altitude from sea level to 30,000 feet, the increase of ζ_m with

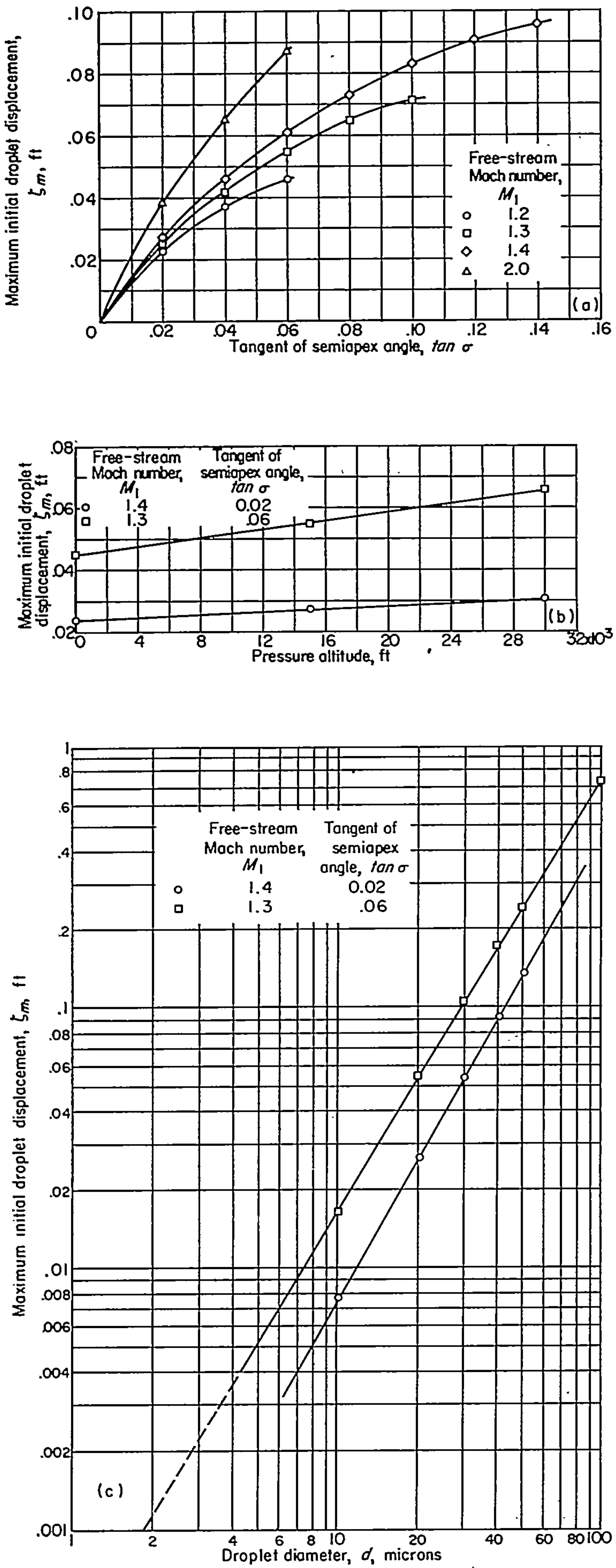

(a) Effect of tangent of semiapex angle. Droplet diameter, 20 microns; pressure altitude, 15,000 feet.
(b) Effect of pressure altitude. Droplet diameter, 20 microns.
(c) Effect of droplet size. Pressure altitude, 15,000 feet.

FIGURE 5.—Total impingement rate W_m for wedge of infinite extent. Free-stream static temperature, 440° R; $W_m = 0.3296 \zeta_m V_1 w$.

an increase in pressure altitude is approximately linear. The variation of ζ_m with the droplet diameter d in microns is shown in figure 5 (c). In the range of droplet diameter from 10 to 100 microns, ζ_m as a function of d results in a curve that is very nearly a straight line when plotted on logarithmic paper. This linearity permits an accurate interpolation of ζ_m when calculations are made for a few droplet diameters for a given value of free-stream Mach number, wedge semiapex angle, and pressure altitude.

Droplet velocities at impingement.—The variation of $V_{d,im}/V_1$ (ratio of droplet impingement velocity to free-stream velocity) with the surface distance along the wedge is presented in figure 6 for three cases. These three cases are representative of the results when the droplet diameter d is 20 microns and the pressure altitude is 15,000 or 30,000 feet. The curves of $V_{d,im}/V_1$ as a function of S have characteristics similar to the curves presenting β as a function of S. At $S=0$, obviously, all the curves have $V_{d,im}/V_1$ equal to unity; and, as S is increased, the value of the velocity ratio rapidly decreases and asymptotically approaches V_2/V_1, the ratio of the air velocity downstream of the shock wave to the air velocity upstream of the shock wave. The solid curve in figure 6 illustrates a typical situation for which V_2/V_1 is very nearly unity ($\tan\sigma=0.02$ and $M_1=2.0$). The two lower curves ($\tan\sigma=0.06$ and 0.10 at $M_1=1.3$) are typical for cases where a stronger shock wave produced by a larger semiapex angle results in decreased values of $V_{d,im}/V_1$ for large values of S.

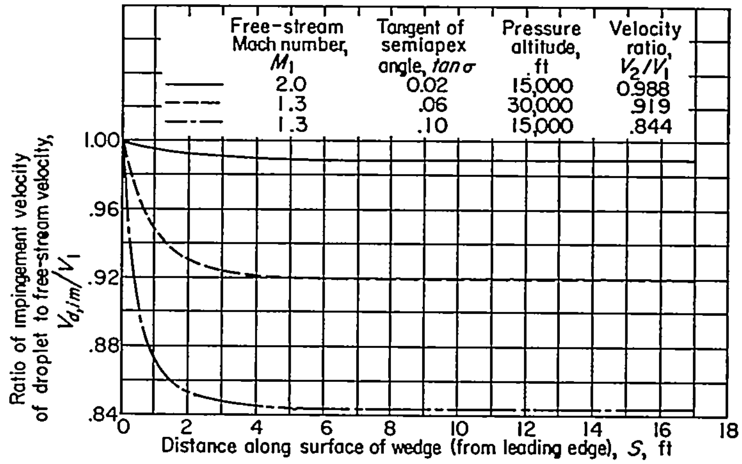

FIGURE 6.—Variation of ratio of impingement velocity of droplet to free-stream velocity with distance along surface of wedge. Free-stream static temperature, 440° R; droplet diameter, 20 microns.

SYMMETRICAL DOUBLE-WEDGE AIRFOIL

As shown in the ANALYSIS, the local impingement efficiency β at any point on the forward surfaces of a double-wedge airfoil (surfaces AB and AC in fig. 3) can be obtained directly from the results for the β against S curves for wedges. The local impingement efficiency β may be obtained from figure 4 or equation (17).

In general, the results for the impingement on a symmetrical double-wedge airfoil are presented in this report in terms of the total collection efficiency E_m as a function of the scale parameter ψ, in an attempt to conform with the existing literature on the impingement characteristics of airfoils. In the notation of the present report, the total collection efficiency E_m as stated in references 7 and 8 is defined as

$$E_m=\frac{|\zeta_u|+|\zeta_l|}{T} \tag{22}$$

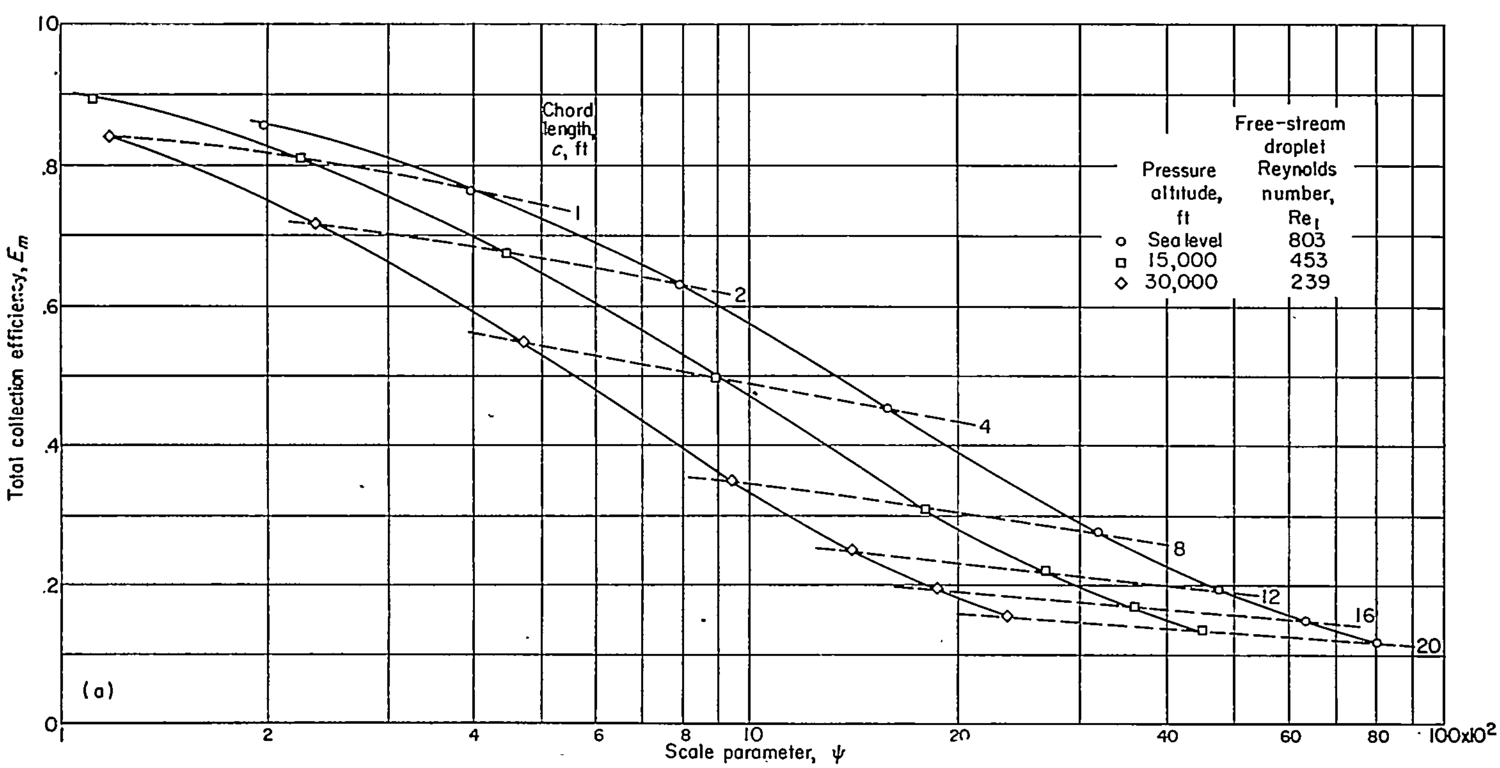

(a) Effect of pressure altitude and chord length. Droplet diameter, 20 microns; free-stream Mach number, 1.4; airfoil thickness ratio, 0.02.

FIGURE 7.—Total collection efficiency of symmetrical double-wedge airfoils as function of scale parameter. Free-stream static temperature, 440° R; angle of attack, 0°.

where T is the maximum thickness of the symmetrical double-wedge airfoil, and $|\zeta_u|$ and $|\zeta_l|$ are the absolute values of the initial displacements from the leading edge (in a direction normal to free-stream direction) of the droplet trajectories that impinge at the shoulder of the upper and lower surfaces, respectively, of the double-wedge airfoil. For the symmetrical double-wedge airfoil at zero angle of attack, $|\zeta_u|$ and $|\zeta_l|$ will be equal; at an angle of attack, the tangent of which is equal to the thickness ratio, the value of $|\zeta_u|$ is equal to zero.

The scale parameter ψ is calculated for the double-wedge airfoil at supersonic speeds as for other airfoils at subsonic speeds. It is defined as

$$\psi=\frac{9c}{a}\frac{\rho_1}{\rho_w} \tag{23}$$

where c is the chord length of the double-wedge airfoil. The results presented for impingement on double-wedge airfoils use essentially the same parameters as used for impingement on wedges—droplet size, free-stream Mach number, double-wedge-airfoil thickness ratio, and pressure altitude. In addition, angle of attack and chord length are specified.

Total collection efficiency at zero angle of attack.—The variation of the total collection efficiency E_m with the scale parameter ψ is presented in figure 7 for a symmetrical double-wedge airfoil at free-stream static temperature of 440° R and zero angle of attack. The effect of pressure altitude on the variation of E_m with ψ for a symmetrical double-wedge airfoil of 0.02 thickness ratio is given in figure 7 (a) for droplet diameter of 20 microns and free-stream Mach number of 1.4. The pressure altitudes presented in the figure are sea level, 15,000, and 30,000 feet. The lines for constant values of chord length from 1 to 20 feet are also included in the figure. For the double-wedge airfoil subjected to a constant-velocity supersonic flow field, the total collection efficiency E_m increases slightly as the pressure altitude is increased when the chord length and the other variables are held constant. Considering E_m as a function of scale parameter ψ where the droplet free-stream Reynolds number Re_1 is held constant yields results similar to those for airfoils having rounded leading edges at subsonic speeds. With Re_1 held constant, the value of E_m decreases as ψ increases in the manner indicated in figure 7 (a). As previously mentioned, the total collection efficiency and the impingement rate at zero angle of attack for a symmetrical double-wedge airfoil are compared in appendix C with those for an NACA 0006–64 airfoil.

The effect of airfoil thickness ratio on the variation of E_m with ψ is presented in figure 7 (b) for thickness ratios from 0.02 to 0.14, droplet diameter of 20 microns, free-stream Mach number of 1.4, and pressure altitude of 15,000 feet. The droplet free-stream Reynolds number is maintained at a value of 453 for all the curves. The effect of increasing the airfoil thickness ratio is to decrease the total collection efficiency. The rate of decrease in E_m with an increase in airfoil thickness ratio becomes somewhat smaller as the thickness ratio increases.

The effect of free-stream Mach number on the variation of total collection efficiency E_m with scale parameter ψ is shown in figure 7 (c) for free-stream Mach numbers of 1.1, 1.2, 1.3, 1.4, 1.5, and 2.0, droplet diameter of 20 microns, airfoil thickness ratio of 0.02, and pressure altitude of 15,000 feet. The results show that the total collection efficiency increases as the free-stream Mach number increases. However, the increase in the total collection efficiency from the free-stream Mach number of 1.1 to 1.2 is considerably greater than the increase in efficiency from a Mach number of 1.2 to 1.3 and from 1.3 to 1.4, and so forth. Calculations for thickness ratios of 0.04 and 0.06 indicate the same trend. For the 0.02 thickness ratio, the lowest Mach number presented in figure 7 (c) ($M=1.1$) is quite close to the limiting Mach number for shock-wave attachment. Therefore, the rate of decrease of total collection efficiency with decreases in free-stream Mach number increases as the Mach number approaches the shock-wave-attachment Mach number as a limit.

The effects of droplet size and chord length on the variation of E_m with ψ are shown in figures 7 (d) and (e). Figure 7 (d) presents curves of E_m against ψ for a symmetrical double-wedge airfoil of 0.02 thickness ratio at a free-stream Mach number of 1.4 and a pressure altitude of 15,000 feet. The curves are for constant values of droplet diameter ($d=$ 10, 20, 30, 40, and 50 microns) as well as for constant values of chord length ($c=1$, 2, 4, 8, and 20 ft). Increasing the droplet size greatly increases the total collection efficiency. For example, at $c=8$ feet, the values of E_m are 0.096, 0.310, 0.495, 0.625, and 0.711 at droplet diameters of 10, 20, 30, 40, and 50 microns, respectively. The rate of increase in the total collection efficiency as the droplet diameter increases is less for the larger droplet sizes. This effect can also be observed in figure 7 (e), in which curves of E_m as a function of ψ are presented for a symmetrical double-wedge airfoil of 0.06 thickness ratio for droplet diameters of 2, 10, 20, 30, 40, 50, and 100 microns, free-stream Mach number of 1.3, and pressure altitude of 15,000 feet.

A comparison of figures 7 (b) and (c) (same droplet size and pressure altitude) shows that the effect on the total collection efficiency E_m of an increase in the free-stream Mach number from 1.1 to 2.0 is, in general, of the same order of magnitude as a decrease from 0.14 to 0.02 thickness ratio. For example, for ψ of 1790 ($c=8$ ft) in figure 7 (b), the values of E_m decreased from 0.310 to 0.165 for an increase from a 0.02 to a 0.14 thickness ratio, respectively, a decrease of 0.145 in the value of E_m. For ψ of 1790 ($c=8$ ft) in figure 7 (c), the values of E_m increased from 0.230 to 0.400 for an increase in the free-stream Mach number from 1.1 to 2.0, respectively, an increase of 0.170 in the value of E_m.

Another comparison of figures 7 (c) and (d) (same airfoil thickness ratio and pressure altitude) shows that the effect on the total collection efficiency E_m of an increase in the droplet diameter from 10 to 50 microns is much greater than an increase in the free-stream Mach number from 1.1 to 2.0. For example, for $c=8$ feet in figure 7 (d), the value of E_m increased from 0.095 to 0.710 for an increase in the droplet diameter from 10 to 50 microns, an increase of 0.615 in the value of E_m. As stated previously, for $c=8$ feet ($\psi=1790$) in figure 7 (c), the increase in the value of E_m is 0.170 for a corresponding increase in the value of the free-stream Mach number from 1.1 to 2.0. For a constant value of

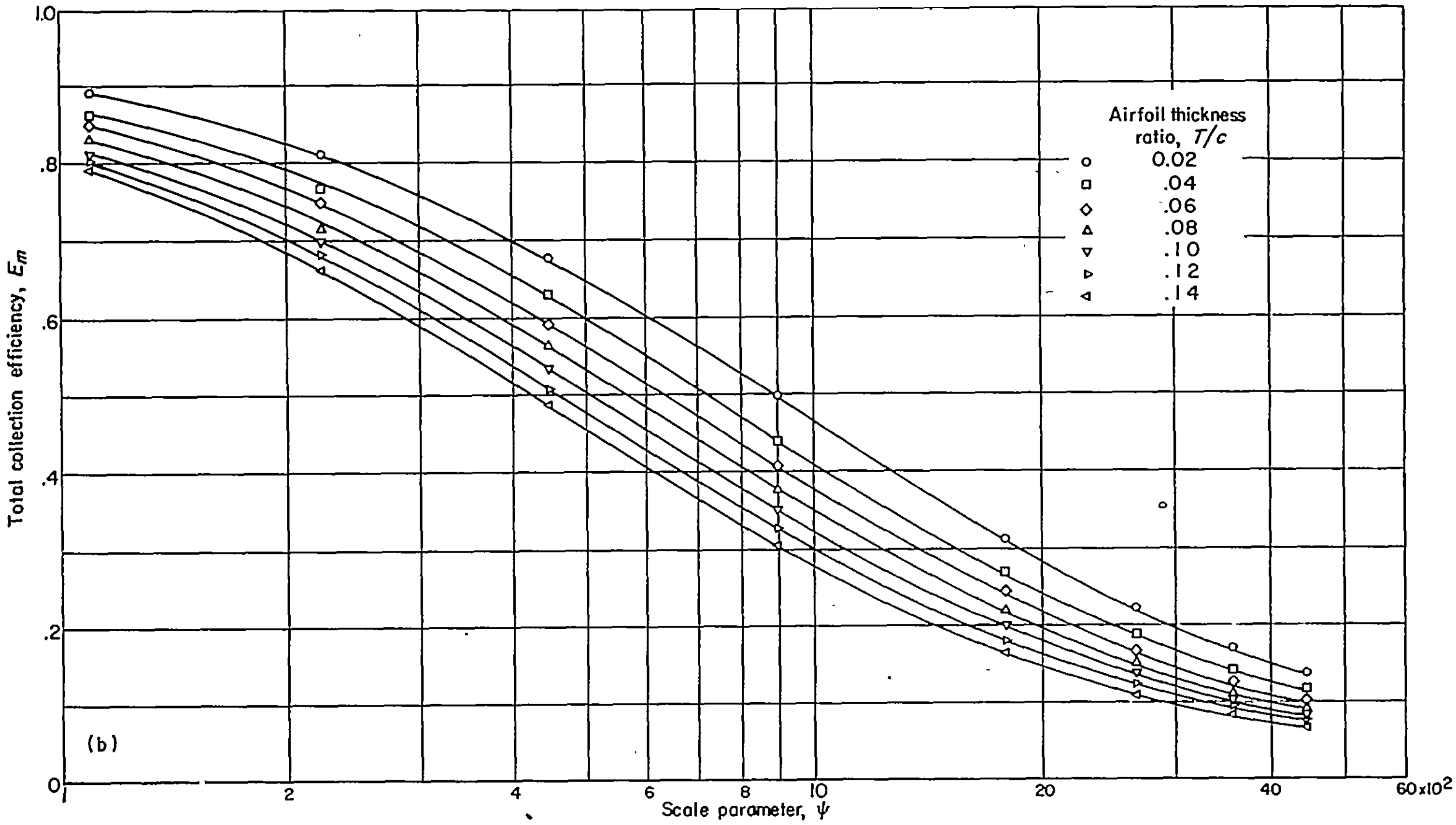

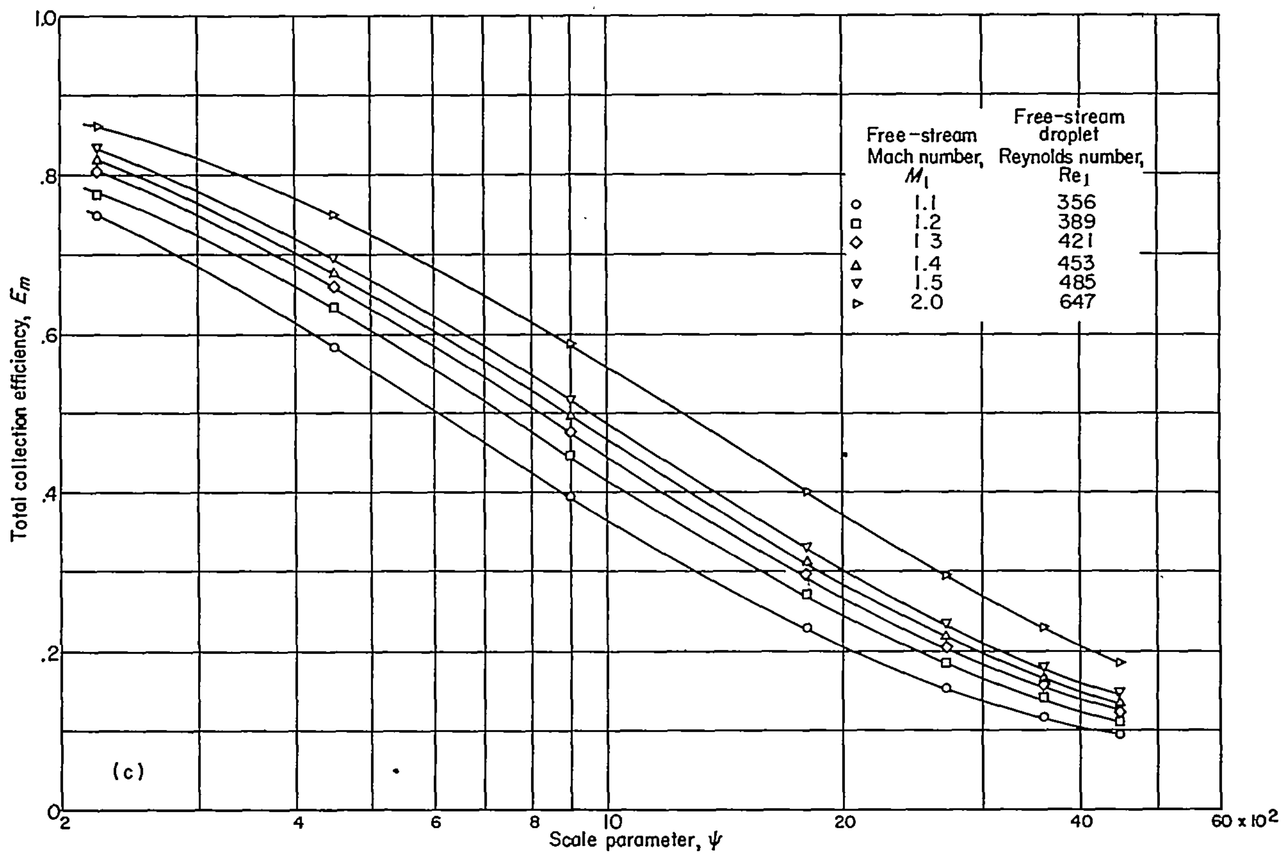

(b) Effect of thickness ratio. Droplet diameter, 20 microns; free-stream Mach number, 1.4; pressure altitude, 15,000 feet; free-stream droplet Reynolds number, 453.

(c) Effect of free-stream Mach number. Droplet diameter, 20 microns; airfoil thickness ratio, 0.02; pressure altitude, 15,000 feet.

FIGURE 7.—Continued. Total collection efficiency of symmetrical double-wedge airfoils as function of scale parameter. Free-stream static temperature, 440° R; angle of attack, 0°.

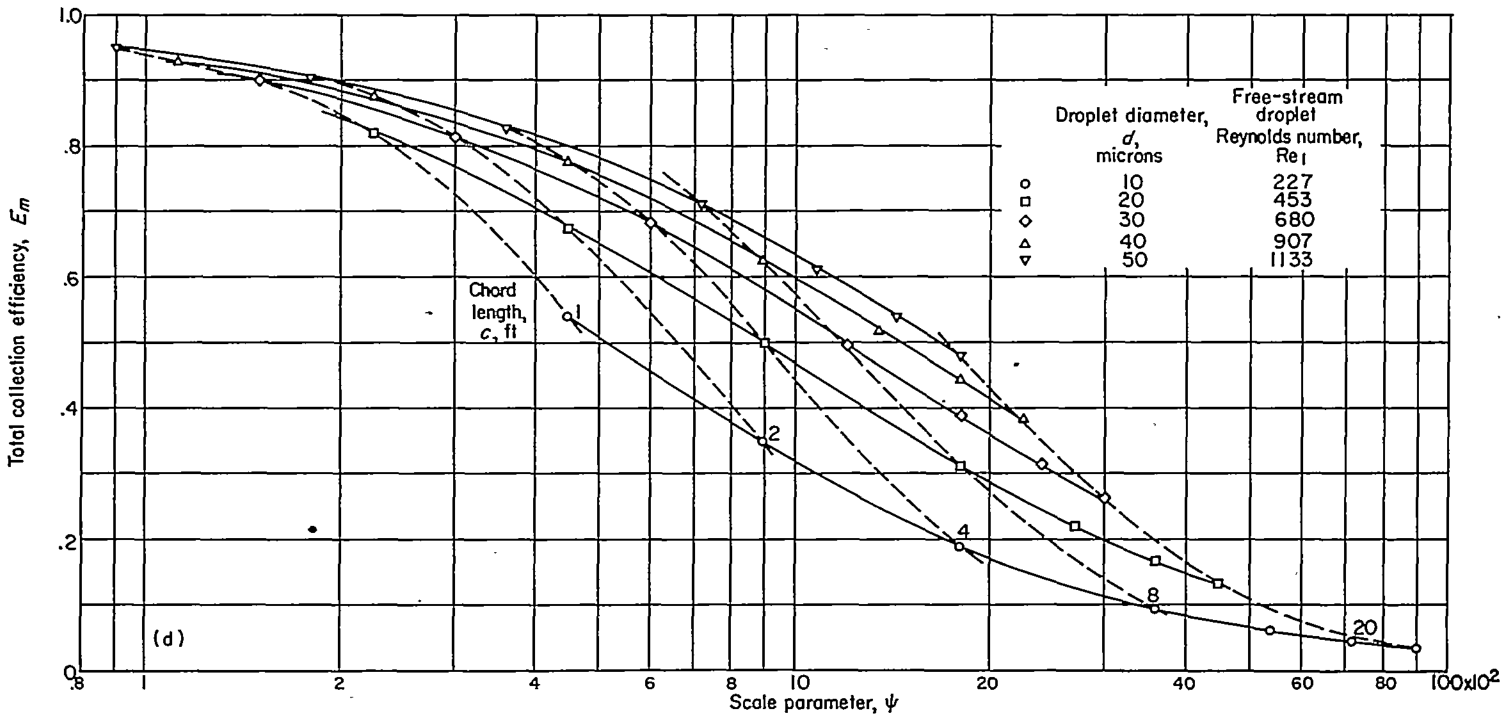

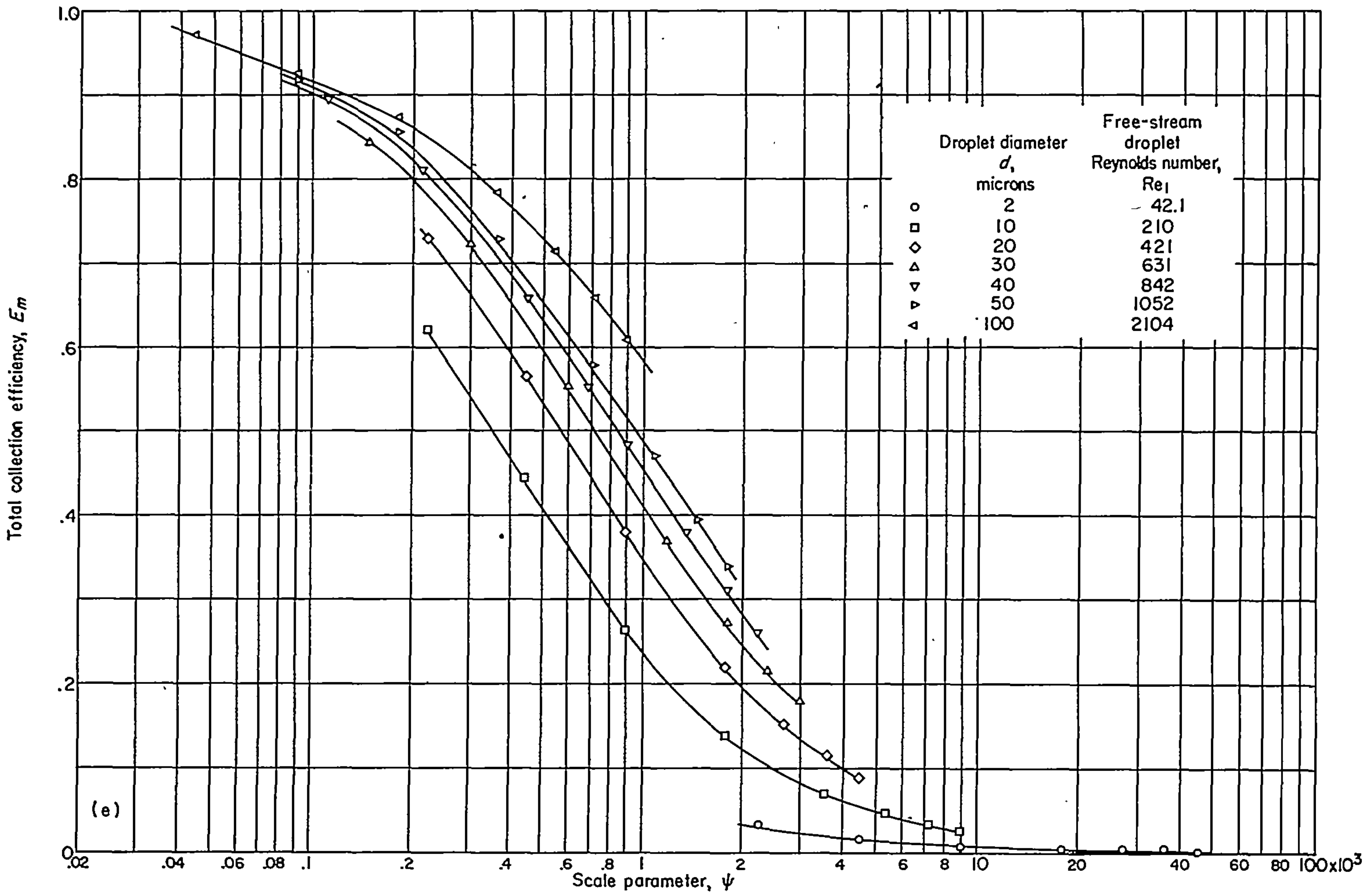

(d) Effect of droplet size and chord length. Free-stream Mach number, 1.4; airfoil thickness ratio, 0.02; pressure altitude, 15,000 feet.
(e) Effect of droplet size. Free-stream Mach number, 1.3; airfoil thickness ratio, 0.06; pressure altitude, 15,000 feet.

FIGURE 7.—Concluded. Total collection efficiency of symmetrical double-wedge airfoils as function of scale parameter. Free-stream static temperature, 440° R; angle of attack, 0°.

chord length, varying the pressure altitude has a relatively small effect on the total collection efficiency (fig. 7 (a)).

Total collection efficiency as function of angle of attack.—The previous discussion is concerned with the total collection efficiencies for the double-wedge airfoil at zero angle of attack only. The effect of angle of attack on the total collection efficiency is presented in figure 8 for airfoil thickness ratios from 0.01 to 0.08, droplet diameter of 20 microns, free-stream Mach number of 1.4, pressure altitude of 15,000 feet, and chord lengths of 1, 2, 4, and 12 feet. The range of angle of attack is from zero to $\tan^{-1}(T/c)$.

The total collection efficiency decreases slightly as the angle of attack increases. The slope of the curve of E_m against $\tan \alpha$ is zero at $\alpha=0$, by virtue of the symmetry of the double-wedge airfoil. As the angle of attack increases, the slope of the E_m against $\tan \alpha$ curve becomes negative, the rate of change becoming more pronounced as the angle of attack increases. The effect of increasing the chord length of the double-wedge airfoil is to decrease slightly the rate of decrease of E_m with respect to $\tan \alpha$. A significant point that is well-illustrated in figure 8 is that, for a constant value of chord length, there apparently exists an envelope of the family of E_m against $\tan \alpha$ curves that have the airfoil thickness ratio T/c as the parameter. This envelope curve presents, in terms of the angle of attack, the maximum total collection efficiency that can be obtained for a symmetrical double-wedge airfoil of any thickness ratio, where the droplet size, free-stream Mach number, pressure altitude, and chord length are considered to be constant.

For the double-wedge airfoil at a free-stream Mach number greater than the shock-wave-attachment Mach number, the decrease in total collection efficiency with an increase in angle of attack is opposed to the trend experienced by rounded-leading-edge airfoils at subsonic Mach numbers (irrespective of the symmetry of the airfoil). For the latter type of airfoil at subsonic speeds, the increase in total collection efficiency (as defined herein) with increasing angle of attack is accounted for by the greatly increased impingement that occurs on the lower surfaces of these airfoils at angle of attack. The reduction of impingement occurring on the upper surfaces of these airfoils at angle of attack is more than balanced by the increased impingement occurring on the lower surfaces. On the other hand, for a given double-wedge airfoil at supersonic speeds with an attached shock wave, the rate of increase with angle of attack of the impingement on the lower surface is less in magnitude than the rate of decrease with angle of attack of the impingement on the upper surface. This general trend for the double-wedge airfoil can be explained with the aid of figure 5 (a), in which the effect of $\tan \sigma$ (tangent of the semiapex angle) on the total impingement rate is presented for a wedge of infinite extent.

The forward upper surface of a symmetrical double-wedge airfoil effectively acts as the finite portion of one surface of an infinite wedge that is decreasing its semiapex angle (effectively the thickness of wedge) as the angle of attack of the double-wedge airfoil increases. The forward lower surface of this type airfoil effectively acts as the finite portion of one surface of an infinite wedge that is increasing its semiapex

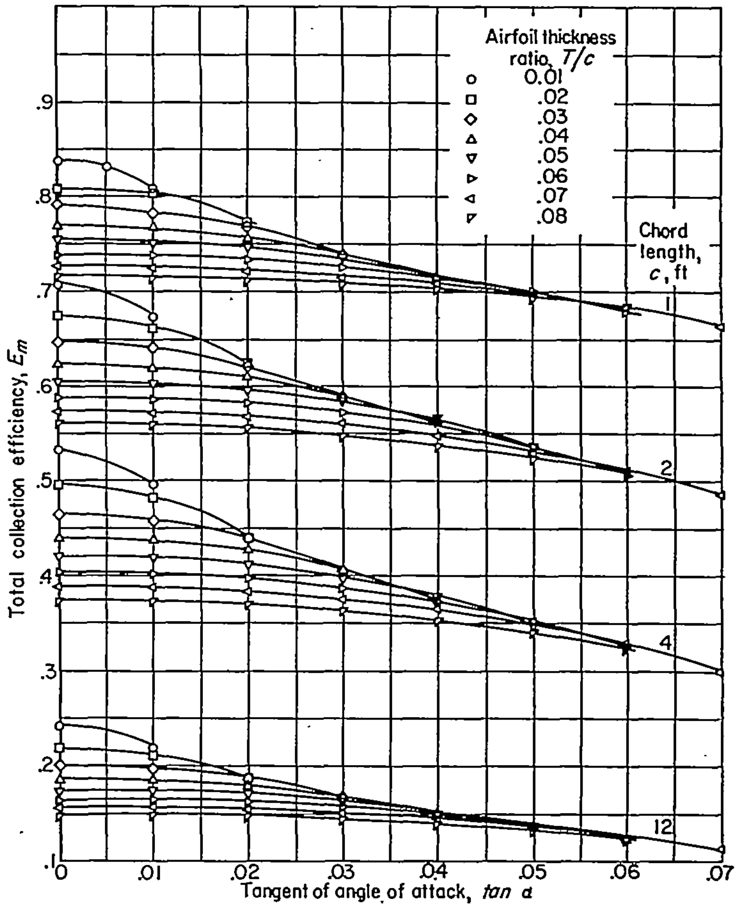

FIGURE 8.—Variation of total collection efficiency of symmetrical double-wedge airfoils with angle of attack. Free-stream static temperature, 440° R; droplet diameter, 20 microns; free-stream Mach number, 1.4; pressure altitude, 15,000 feet.

angle as the angle of attack increases. In figure 5 (a) the increase in ζ_m, which is exactly proportional to the total impingement rate, becomes smaller with an increase in $\tan \sigma$ (i.e., $d^2\zeta_m/d(\tan \sigma)^2<0$) for all possible values of the semiapex angle σ. For example, in figure 5 (a) for the curve of $M_1=1.4$, the impingement on a symmetrical double-wedge airfoil of 0.08 thickness ratio and large chord extent at zero angle of attack would be very nearly proportional to twice the value of ζ_m at $\tan \sigma$ of 0.08 ($2\zeta_m=0.146$ ft). The impingement for the same airfoil under the same conditions and at an angle of attack of 2.291° ($\tan \alpha=0.04$) would be very nearly proportional to the sum of ζ_m at $\tan \sigma$ of 0.04 and 0.12 ($\zeta_{m,u}+\zeta_{m,l}=0.046+0.0905=0.1365$ ft).

Total collection efficiency as function of relative modified inertia parameter.—For air-flow fields that contain a shock wave, such as those considered herein, the water droplets upon crossing the shock wave suddenly have a velocity relative to the air. For the double-wedge airfoil with an attached shock wave, this initial relative velocity is the same for all droplets entering the air-flow field downstream of the shock wave. As discussed in previous sections, this common initial velocity U_i may be considered the initial velocity of projection of a droplet in a reference frame having no air motion in it and moving relative to the fixed frame of reference at the constant velocity of the air downstream of the shock wave. Therefore, it is of interest to define a set of inertia parameters, F and F_0, based on the motion of the droplet in this moving reference frame. The relative inertia parameter based on the relative velocity U_t is defined as

$$F=K\frac{U_t}{V_1}=\frac{2}{9}\frac{\rho_w a^2 U_t}{\mu_1 c}=\frac{x_{m,s}}{c}$$

where K is the inertia parameter in the fixed frame of reference, defined as

$$K=\frac{2}{9}\frac{\rho_w a^2 V_1}{\mu_1 c} \tag{24}$$

and $x_{m,s}$ is that value of the maximum distance of travel obtained when Stokes' law is assumed for the drag force on the droplet.

The relative modified inertia parameter, also based on the relative velocity U_t, is defined as

$$F_0=\frac{x_m}{x_{m,s}}F=\frac{x_m}{c}$$

where x_m is defined in equation (9), and experimental values are used for the drag force on the droplet.

For the problem of water-droplet impingement on airfoils having rounded leading edges at subsonic speeds, it is impossible to define a similar relative modified inertia parameter. Also, for any airfoil at supersonic speeds, it is impossible to define a relative modified inertia parameter, unless the shock wave from the leading edge is of constant strength in the vicinity of the airfoil, as in the case of the double-wedge airfoils with attached shock waves. If the strength of the shock wave is not constant, as for the case of a bow shock wave preceding a blunt obstacle, then the value of F_0 is not constant for all the trajectories of a given droplet size. Thus, the problem of impingement on wedges and double-wedge airfoils at supersonic speeds with attached shock waves is unique in that a relative modified inertia parameter can be defined and used in correlating the total collection efficiencies.

The correlation of the total collection efficiency with the relative modified inertia parameter F_0 is shown in figure 9 (a) for droplet diameters varying from 2 to 100 microns and for pressure altitudes of sea level, 15,000, and 30,000 feet. For the symmetrical double-wedge airfoil of 0.06 thickness ratio at M_1=1.3 and zero angle of attack, the droplet free-stream Reynolds number Re_1 varies from 42.1 to 2104. The values of E_m for a given thickness ratio, Mach number, and angle of attack generally form the basis for a single curve with a small amount of scatter existing in the higher range of value of F_0. In the lower range of F_0, for all values of Re_1 the plotted points have negligible scatter. The small scatter observed is possibly due to the existence of a very slight trend of the curves of E_m against F_0 with Re_1 for the higher values of F_0.

The effect of increasing the thickness ratio is presented in figure 9 (b) for symmetrical double-wedge airfoils of 0.02, 0.06, and 0.12 thickness ratio. Increasing the thickness ratio displaces the E_m against F_0 curve toward larger values

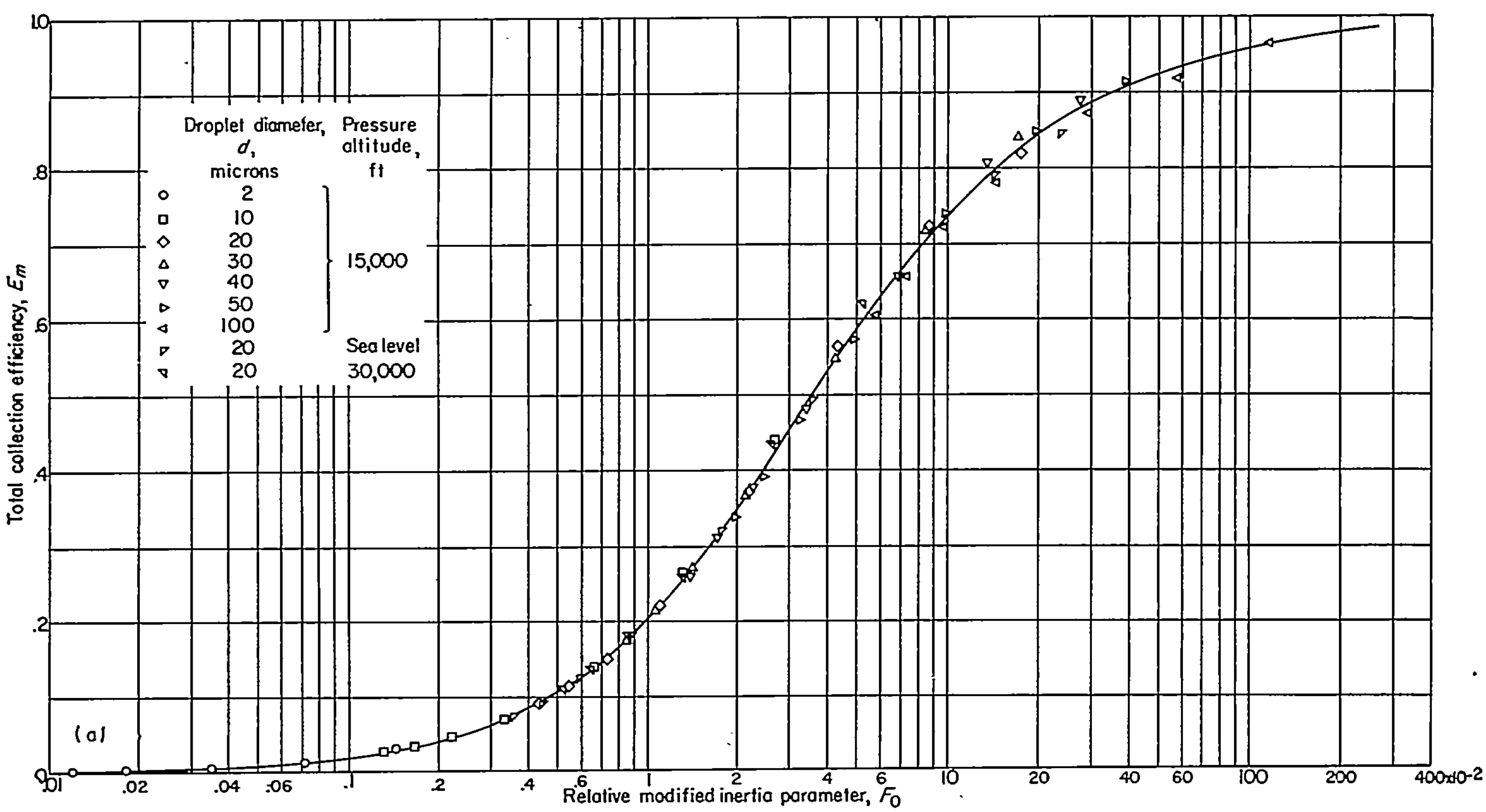

(a) Correlation of pressure altitude and droplet size. Free-stream Mach number, 1.3; airfoil thickness ratio, 0.06.

FIGURE 9.—Total collection efficiency of symmetrical double-wedge airfoils as function of relative modified inertia parameter. Free-stream static temperature, 440° R; angle of attack, 0°.

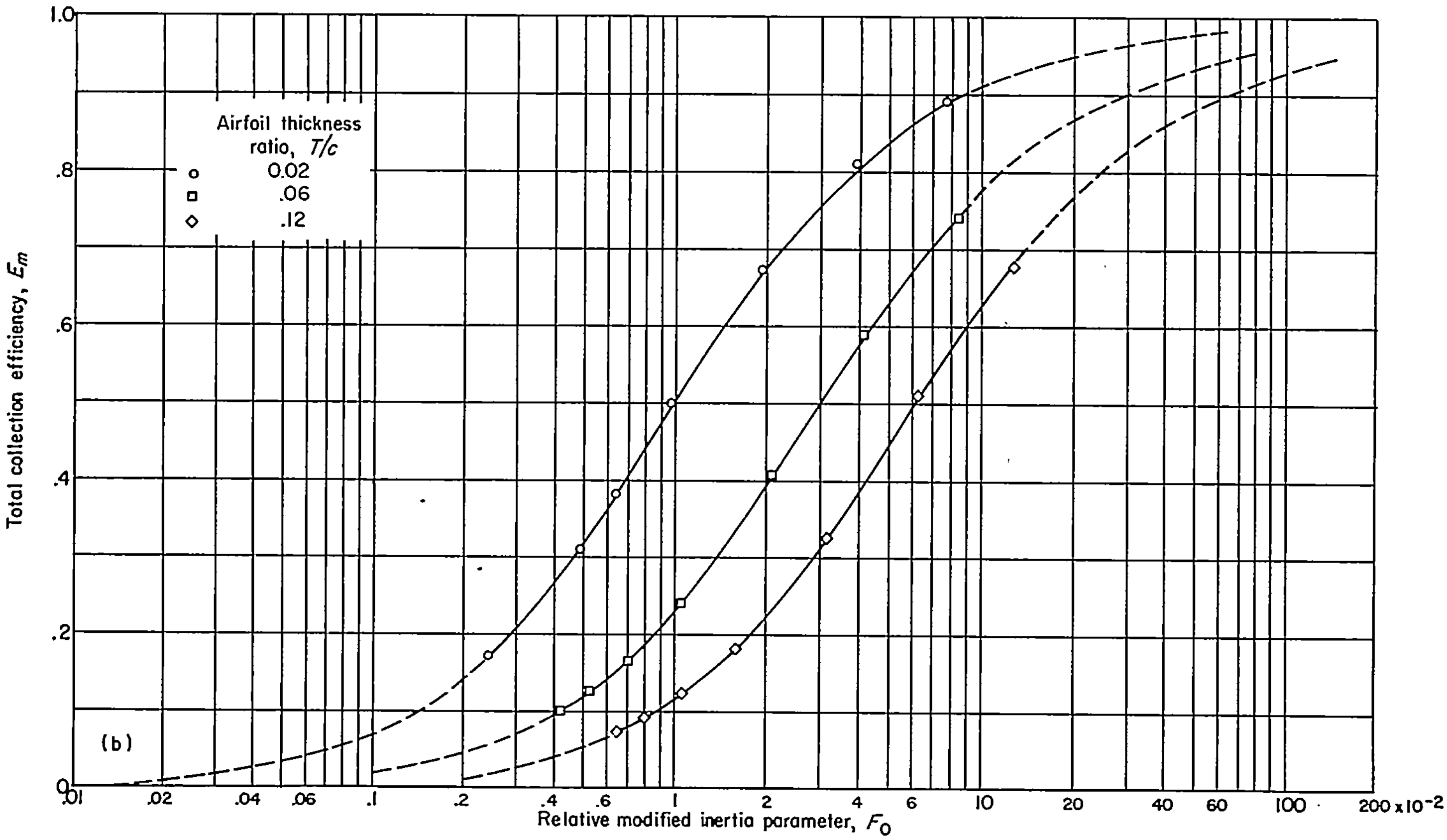

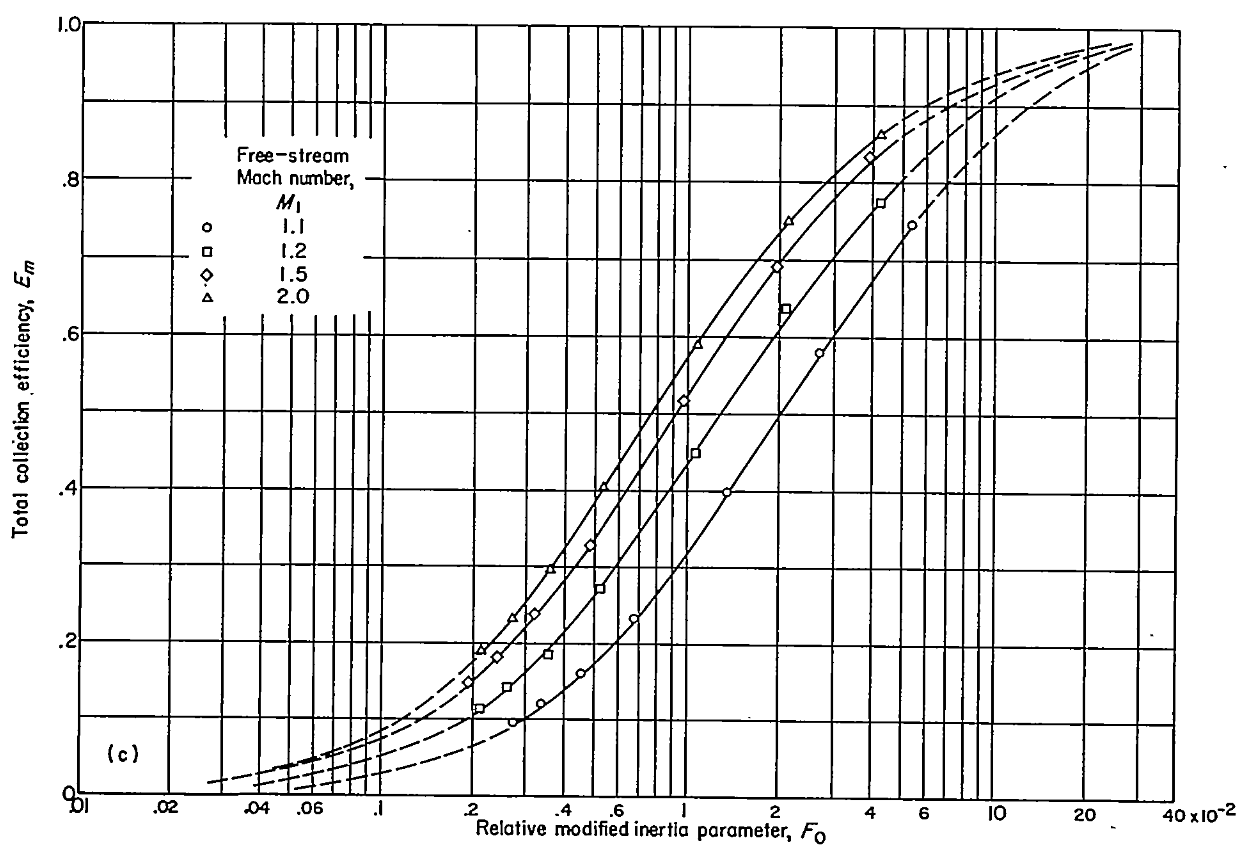

(b) Effect of thickness ratio. Droplet diameter, 20 microns; free-stream Mach number, 1.4; pressure altitude, 15,000 feet.
(c) Effect of free-stream Mach number. Droplet diameter, 20 microns; airfoil thickness ratio, 0.02; pressure altitude, 15,000 feet.

FIGURE 9.—Concluded. Total collection efficiency of symmetrical double-wedge airfoils as function of relative modified inertia parameter. Free-stream static temperature, 440° R; angle of attack, 0°.

of F_0. Changing the thickness ratio of the double-wedge airfoil does not alter the shape of the curve itself.

The effect of the free-stream Mach number on the variation of E_m with F_0 is presented in figure 9 (c) for the symmetrical double-wedge airfoil of 0.02 thickness ratio for droplet diameter of 20 microns, free-stream Mach numbers of 1.1, 1.2, 1.5, and 2.0, and pressure altitude of 15,000 feet. Increasing the Mach number displaces the entire curve of E_m against F_0 toward smaller values of F_0. As the value of M_1 increases, the rate of displacement of the curve with increasing M_1 becomes smaller. The displacement of the curve obtained by increasing the Mach number from 1.1 to 1.2 is more than that obtained by increasing it from 1.2 to 1.5 and from 1.5 to 2.0.

The relative inertia parameter F and the relative modified inertia parameter F_0 of the moving frame of reference correspond, respectively, to the inertia parameter K and a modified inertia parameter K_0 of the fixed frame of reference. The modified inertia parameter is defined in reference 14 as

$$K_0=\frac{\lambda}{\lambda_s}K \tag{25}$$

where λ is the maximum distance of travel of a droplet projected into still air with the free-stream velocity V_1. The term λ_s is the value of the maximum distance of travel λ when Stokes' law is assumed for the drag force on the droplet. The total collection efficiency of a symmetrical double-wedge airfoil is presented in appendix D as a function of the modified inertia parameter K_0.

SUMMARY OF RESULTS

This report presents an analysis of the problem of impingement of water droplets on a wedge and a double-wedge airfoil at supersonic speeds with attached shock waves. When a suitable empirical relation is used for the drag coefficient of a sphere, the analysis allows a closed-form integration of the equations of motion for the water droplets. The integration results in analytical expressions for the equation of the trajectories, the droplet velocity at any point on the trajectories, the local impingement efficiencies, and the total rate of impingement. The results of the calculations of rate, extent, and distribution of impingement of water droplets on wedges and symmetrical double-wedge airfoils are summarized briefly as follows (the Mach number referred to is the free-stream Mach number, which is greater than the attachment Mach number for the wedge or the double-wedge airfoil):

1. At a given value of Mach number, droplet size, and pressure altitude, the local impingement efficiency as a function of the dimensional surface distance is the same for both the wedge and the symmetrical double-wedge airfoil at zero angle of attack, provided the tangent of the semiapex angle of the wedge is equal to the thickness ratio of the symmetrical double-wedge airfoil.

2. For any Mach number, pressure altitude, and droplet diameter, the value of β_0 is equal to the sine of the semiapex angle for wedge or symmetrical double-wedge airfoil. [β_0 is the value (maximum) of local impingement efficiency as distance from leading edge to point of impingement approaches zero.]

3. The effect of the free-stream static temperature on the local impingement efficiency and total collection efficiency is negligible for temperatures from 420° to 460° R.

4. At constant values of Mach number, droplet size, and semiapex angle of the wedge or corresponding thickness ratio of the symmetrical double-wedge airfoil, an increase in the pressure altitude increases slightly the local impingement efficiencies and total collection rates on wedges and symmetrical double-wedge airfoils, but has a negligible effect on the surface extent of perceptible impingement.

5. At constant values of Mach number, droplet size, and pressure altitude, increasing the thickness ratio of the symmetrical double-wedge airfoil or corresponding semiapex angle of the wedge increases the local impingement efficiency, has a negligible effect on the surface extent of perceptible impingement, and decreases the total collection efficiency of the symmetrical double-wedge airfoil.

6. At constant values of droplet size, pressure altitude, and semiapex angle of the wedge or thickness ratio of the symmetrical double-wedge airfoil, an increase in Mach number increases both the surface extent of impingement and the value of the local impingement efficiency.

7. At constant values of pressure altitude, semiapex angle of the wedge or thickness ratio of the symmetrical double-wedge airfoil, and Mach number, an increase in the droplet size increases considerably the surface extent of perceptible impingement, the local impingement efficiency, and the total impingement rate.

8. The variation of total collection efficiency of the symmetrical double-wedge airfoil at zero angle of attack as a function of the scale parameter for constant values of the droplet free-stream Reynolds number is similar in form to that for subsonic airfoils.

9. The total collection efficiency of the symmetrical double-wedge airfoil decreases slightly as the angle of attack increases.

10. For a symmetrical double-wedge airfoil of a given thickness ratio and Mach number, the values of total collection efficiency for a wide range of values of droplet free-stream Reynolds number comprise a single curve when plotted against the relative modified inertia parameter. The effect of increasing the thickness ratio or decreasing the Mach number is to displace the entire curve in the direction of larger values of relative modified inertia parameter.

LEWIS FLIGHT PROPULSION LABORATORY
NATIONAL ADVISORY COMMITTEE FOR AERONAUTICS
CLEVELAND, OHIO, *April 21, 1953*

APPENDIX A

SYMBOLS

The following symbols are used in this report:

a droplet radius, ft
C_D drag coefficient, dimensionless
c airfoil chord length, ft
D drag force on spherical water droplet, lb
d droplet diameter, microns
E_m total collection efficiency (defined by eq. (22)), dimensionless
F relative inertia parameter, $\frac{2}{9}\frac{\rho_w a^2 U_i}{\mu_1 c}=\frac{x_{m,s}}{c}$, dimensionless
F_0 relative modified inertia parameter, $\frac{x_m}{x_{m,s}}F=\frac{x_m}{c}$
g acceleration due to gravity, 32.2 ft/sec^2
K inertia parameter, $\frac{2}{9}\frac{\rho_w a^2 V_1}{\mu_1 c}=\frac{\lambda_s}{c}$, dimensionless
K_0 modified inertia parameter, $\frac{\lambda}{\lambda_s}K=\frac{\lambda}{c}$, dimensionless
M Mach number
m empirical constant (used in eq. (5)), 2/3
n_1, n_2, n_3 constants of flow field (defined by eqs. (18a), (18b), and (18c), respectively)
p static pressure, lb/sq ft
R gas constant, 53.3 ft-lb/(lb)(°F)
Re_r droplet Reynolds number relative to air behind shock wave, $2a\rho_2 U/\mu_2$, dimensionless
Re_1 free-stream droplet Reynolds number, $2a\rho_1 V_1/\mu_1$, dimensionless
S distance to point of impingement measured from leading edge for water droplet that enters flow field behind shock wave at distance ζ above leading edge (eq. (15) and fig. 1), ft
T maximum thickness of airfoil, ft
t time, sec
t_1 free-stream static temperature, °R
U magnitude of droplet velocity relative to air velocity downstream of shock wave, $|\overline{V}_d-\overline{V}_2|$, fps
V velocity, fps or mph
W rate of water catch, lb/(hr)(ft span)
W_β local rate of water catch, lb/(hr)(sq ft surface)
w liquid-water content of air, g/cu m
x $\int_0^t U\,dt$, displacement of droplet in moving frame of reference (relative to air stream); where $t=0$ the instant water droplet intercepts shock wave
x_m maximum value of displacement x as $\tau\rightarrow\infty$ as limit (maximum distance of travel of droplet projected into still air with relative velocity U_i), ft
$x_{m,s}$ value of maximum distance of travel x_m obtained by assuming Stokes' law for drag force on droplet, ft
α angle of attack of airfoil, deg
β local impingement efficiency, $d\zeta/dS$, dimensionless
β_0 maximum value of β as $S\rightarrow 0$; $\beta_0\equiv\sin\sigma$, dimensionless
γ ratio of specific heats (1.4 for air)
ϵ empirical constant (used in eq. (5)), 0.158, dimensionless
ζ initial displacement of droplet trajectories from leading edge in direction normal to free-stream direction (eq. (13))
ζ_m maximum value of initial droplet displacement ζ obtained when trajectory is tangent to wedge surface (theoretically as $S\rightarrow\infty$)
$|\zeta_u|$, $|\zeta_l|$ absolute values of initial displacement from leading edge (in direction normal to free-stream direction) of droplet trajectories that impinge at shoulder of upper and lower surfaces, respectively, of double-wedge airfoil
η distance along shock wave measured from wedge apex to point where droplet trajectory intercepts shock wave
θ shock-wave angle
κ angle between free-stream velocity vector $\overline{V}_1$ and droplet velocity vector $\overline{V}_d$
λ maximum distance of travel of droplet projected into still air with free-stream velocity V_1, ft
λ_s value of distance of travel λ obtained by assuming Stokes' law for drag force on water droplet, ft
μ dynamic viscosity based on static temperature, (lb)(sec)/sq ft
ν angle between free-stream velocity vector $\overline{V}_1$ and initial relative velocity vector $\overline{U}_i$ (defined by eq. (13a))
ξ, ξ' components of droplet displacement referred to wedge surface (defined by eq. (12)), ft
ρ mass density of air, slugs/cu ft
ρ_w water-droplet mass density, 1.9398 slugs/cu ft
σ semiapex angle
σ' angle between droplet velocity vector $\overline{V}_d$ and velocity vector $\overline{V}_2$
τ dimensionless time variable, $(3\mu_2/\rho_w a^2)t$
φ phase angle, $\tan^{-1}(Re_{r,i}^{-1/3}\epsilon^{-1/2})$, $0\leqq\varphi\leqq\frac{\pi}{2}$ (eq. (9))
ψ scale parameter, $(9c/a)(\rho_1/\rho_w)$
Ω ratio of air velocity downstream of shock wave to free-stream velocity V_2/V_1
ω ratio of initial droplet relative velocity to free-stream velocity U_i/V_1

Subscripts:

d droplet
i initial (at shock wave)
im impingement
l lower
m maximum
u upper
1 free stream
2 downstream of shock wave (in fixed frame of reference)

Barred symbols denote vectorial quantities.

APPENDIX B

CLOSED-FORM INTEGRATION OF EQUATION OF MOTION (RELATIVE TO AIR FLOW DOWNSTREAM OF SHOCK WAVE)

The various steps necessary to the closed-form integration of equation (6), which is the differential equation of motion of the water droplet in the moving reference frame, are given herein. The differential equation of motion (6) can be rewritten as

$$\frac{dU}{dt}=-\frac{A_2}{A_1}\frac{24U}{a^2}(1+\epsilon A_1^m U^m a^m) \quad \text{(B1)}$$

where, for convenience,

$$Re_r=A_1Ua \quad \text{(B2)}$$

$$A_1=\frac{2\rho_2}{\mu_2} \quad \text{(B3)}$$

$$A_2=\frac{3}{8}\frac{\rho_2}{\rho_w} \quad \text{(B4)}$$

Algebraic simplification and rewriting result in the form

$$dt=-\frac{A_3\,dU}{U(1+A_4U^m)} \quad \text{(B5)}$$

where

$$A_3=\frac{A_1}{A_2}\frac{a^2}{24} \quad \text{(B6)}$$

and

$$A_4=\epsilon A_1^m a^m \quad \text{(B7)}$$

Equation (B5) is not readily integrable in its present form. By letting

$$p=U^m \quad \text{(B8)}$$

and

$$p'=\frac{p}{p_i}=\frac{U^m}{U_i^m} \quad \text{(B9)}$$

equation (B5) becomes

$$dt=-\frac{A_3}{m}\frac{dp'}{p'}+\frac{A_3}{m}\frac{A_4p_i\,dp'}{1+A_4p_ip'} \quad \text{(B10)}$$

This form of the equation is readily integrated, and upon resubstituting the relations (B8) and (B9), there is obtained the following expression for the velocity of the droplet as a function of the time t:

$$U=U_i\left\{\exp\left[(t-B_1)\frac{m}{A_3}\right]-U_i^mA_4\right\}^{-1/m} \quad \text{(B11)}$$

where B_1 is the constant of integration.

Since $U\equiv\frac{dx}{dt}$, equation (B11) can be rewritten in integral form as

$$\int dx=\int U_i\left\{\exp\left[(t-B_1)\frac{m}{A_3}\right]-U_i^mA_4\right\}^{-1/m}dt+B_2 \quad \text{(B12)}$$

where B_2 is the second integration constant. Equation (B12) requires simplification before a closed-form integration can be performed. Consider the following substitutions:

$$y=\frac{m}{A_3}t \quad \text{(B13)}$$

$$A_5=\frac{A_3}{m}U_i(U_i^mA_4)^{-1/m}=\frac{A_3}{m}(A_4)^{-1/m} \quad \text{(B14)}$$

$$A_6=(U_i^mA_4)^{-1}\exp\left[-B_1m/A_3\right] \quad \text{(B15)}$$

By using the substitutions given by (B13), (B14), and (B15), it is possible to write equation (B12) as

$$\int dx=\int A_5(A_6e^y-1)^{-1/m}dy+B_2 \quad \text{(B16)}$$

Before further steps can be taken in the closed-form integration of the equation of motion of the droplet, the value of the empirical constant m must be determined. It is noted that in approximating the curve of the drag coefficient as a function of the local Reynolds number by a relation of the form given by

$$C_D=\frac{24}{Re_r}(1+\epsilon Re_r^m) \quad (5)$$

it is possible to consider that the value of m is 2/3 and the value of ϵ is 0.158. That the approximation of the experimental curve by the empirical relation is very good in the range of Reynolds numbers from about 0.5 to 500 can be seen by referring to figure 2, which presents a graph of the empirical relation along with the drag-coefficient data of references 4 and 12.

The use of $m=2/3$ in equation (B16) along with the substitution

$$e^y=q \quad \text{(B17)}$$

and the use of formulas of integration given on pages 16 and 17 of reference 15 allow equation (B16) to be integrated as shown in the following steps:

$$\int dx=\int\frac{A_5dq}{q(A_6q-1)^{3/2}}+B_2$$

$$\int dx=-\int\frac{A_5dq}{q(A_6q-1)^{1/2}}+A_6\int\frac{A_5dq}{(A_6q-1)^{3/2}}+B_2$$

$$\frac{x-B_2}{2A_5}=-\frac{1}{\sqrt{A_6q-1}}-\tan^{-1}\sqrt{A_6q-1} \quad \text{(B18)}$$

If the original time or independent variable t is reintroduced into equation (B18) and the substitutions are made for A_5 and A_6, the equation has the form

$$\frac{(A_4)^{3/2}(B_2-x)}{3A_3}=\frac{(A_4U_i^{2/3})^{1/2}}{\sqrt{\exp\left[\frac{2(t-B_1)}{3A_3}\right]-A_4U_i^{2/3}}}+$$

$$\tan^{-1}\left\{\frac{1}{(U_i^{2/3}A_4)^{1/2}}\sqrt{\exp\left[\frac{2(t-B_1)}{3A_3}\right]-A_4U_i^{2/3}}\right\} \quad \text{(B19)}$$

Substituting for A_3 and A_4 (except in the exponent of e) in equation (B19) results in

$$\frac{B_2-x}{a}\left(3\epsilon^{3/2}\frac{\rho_2}{\rho_w}\right)=\frac{Re_{r,i}{}^{1/3}\epsilon^{1/2}}{\sqrt{\exp\left[\frac{2(t-B_1)}{3A_3}\right]-Re_{r,i}{}^{2/3}\epsilon}}+$$

$$\tan^{-1}\left\{\frac{1}{Re_{r,i}{}^{1/3}\epsilon^{1/2}}\sqrt{\exp\left[\frac{2(t-B_1)}{3A_3}\right]-Re_{r,i}{}^{2/3}\epsilon}\right\} \quad \text{(B20)}$$

Equation (B20) is the integrated equation with undetermined integration constants for the motion of the water droplets relative to the air velocity behind the shock wave. The integration constants are determined from the boundary conditions, which are

$$\left.\begin{matrix} U=U_i \\ x=0 \end{matrix}\right\}\text{at } t=0$$

The substitution of the boundary conditions, and thus the determination of the integration constants B_1 and B_2, results in the final form of the integrated equation of motion for the water droplets relative to the air velocity downstream of the shock wave as follows (in the frame of reference moving with the constant velocity V_2):

$$x=\frac{a}{3}\epsilon^{-3/2}\frac{\rho_w}{\rho_2}\left[Re_{r,i}{}^{1/3}\epsilon^{1/2}+\tan^{-1}(Re_{r,i}{}^{-1/3}\epsilon^{-1/2})-\frac{1}{\sqrt{(Re_{r,i}{}^{-2/3}\epsilon^{-1}+1)e^{\tau}-1}}-\tan^{-1}\sqrt{(Re_{r,i}{}^{-2/3}\epsilon^{-1}+1)e^{\tau}-1}\right] \quad (7)$$

The final form of the corresponding equation for the relative velocity of the water droplet as a function of the dimensionless time variable is obtained from equation (B11) as

$$U=\frac{U_i}{Re_{r,i}\epsilon^{3/2}}\left[(Re_{r,i}{}^{-2/3}\epsilon^{-1}+1)e^{\tau}-1\right]^{-3/2} \quad (8)$$

It can be seen from equations (7) and (8) that as t approaches infinity the value of U approaches zero and that a limit exists for the value of x as t approaches infinity. This limiting value of x is

$$x_m=\frac{a}{3}\epsilon^{-3/2}\frac{\rho_w}{\rho_2}\left(Re_{r,i}{}^{1/3}\epsilon^{1/2}-\frac{\pi}{2}+\varphi\right) \quad (9)$$

where

$$\varphi=\tan^{-1}(Re_{r,i}{}^{-1/3}\epsilon^{-1/2});\ 0\leq\varphi\leq\frac{\pi}{2}$$

APPENDIX C

COMPARISON OF COLLECTION EFFICIENCY AND IMPINGEMENT RATE FOR SYMMETRICAL DOUBLE-WEDGE AIRFOIL WITH THOSE FOR NACA 0006-64 AIRFOIL

A comparison of the total collection efficiency as a function of a modified inertia parameter K_0 for a symmetrical double-wedge airfoil at supersonic speeds (attached shock wave) with that for the NACA 0006-64 airfoil (ref. 9) at free-stream Mach numbers less than critical is presented in figure 10. Both airfoils have 0.06 thickness ratios and are at zero angle of attack. It is important to keep in mind that figure 10 does not allow a comparison of the two airfoils at the same Mach number, and such a comparison cannot be made, because the analysis for the NACA 0006-64 airfoil is not valid above the critical Mach number and that for the symmetrical double-wedge airfoil is not valid below the shock-wave-attachment Mach number. It is, however, of value to consider a comparison of the two airfoils with each operating within its appropriate speed range. In figure 10 the rate of increase in E_m with respect to K_0 is greater for the symmetrical double-wedge airfoil than for the NACA 0006-64. For a constant droplet size, pressure altitude and temperature, and free-stream Mach number, resulting in a constant value of λ, K_0 varies inversely as the chord length ($K_0=\lambda/c$). In general, therefore, the rate of decrease in E_m with increasing chord length is greater in magnitude for the symmetrical double-wedge airfoil than for the NACA 0006-64 airfoil.

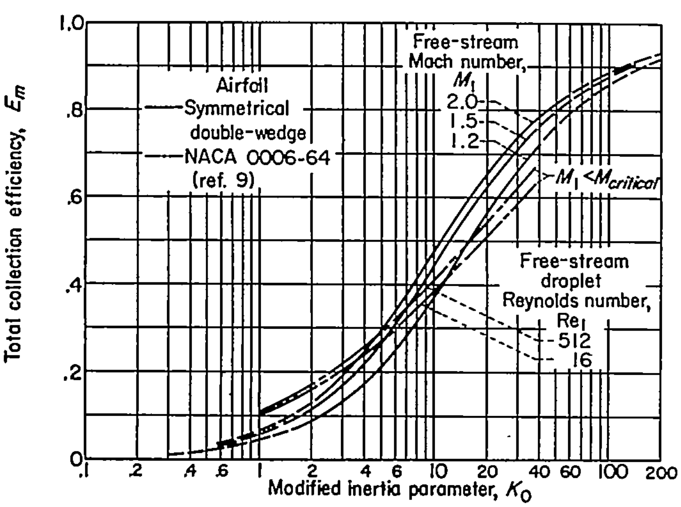

FIGURE 10.—Comparison of total collection efficiency as function of modified inertia parameter for symmetrical double-wedge airfoil at supersonic speeds with attached shock wave with that for NACA 0006-64 airfoil at free-stream Mach number less than critical. Airfoil thickness ratio, 0.06; angle of attack, 0°.

A comparison of the rate of total water catch per unit span for the symmetrical double-wedge airfoil with that for the NACA 0006-64 airfoil can be obtained if values (necessarily different) for the free-stream Mach numbers for the two airfoils are assigned. Assume that both airfoils are of the same thickness ratio and chord length and that they encounter identical icing conditions of droplet diameter (20 microns), pressure altitude and temperature (15,000 ft and 440° R), and liquid-water content (0.5 g/cu m), but have free-stream Mach numbers of 1.5 and 0.75, respectively. For the static temperature assumed, the Mach numbers of 1.5 and 0.75 correspond to speeds of 1051 and 526 miles per hour, respectively. Therefore, the magnitudes of the inertia parameter K and the free-stream droplet Reynolds number Re_1 for the double-wedge airfoil are twice as great

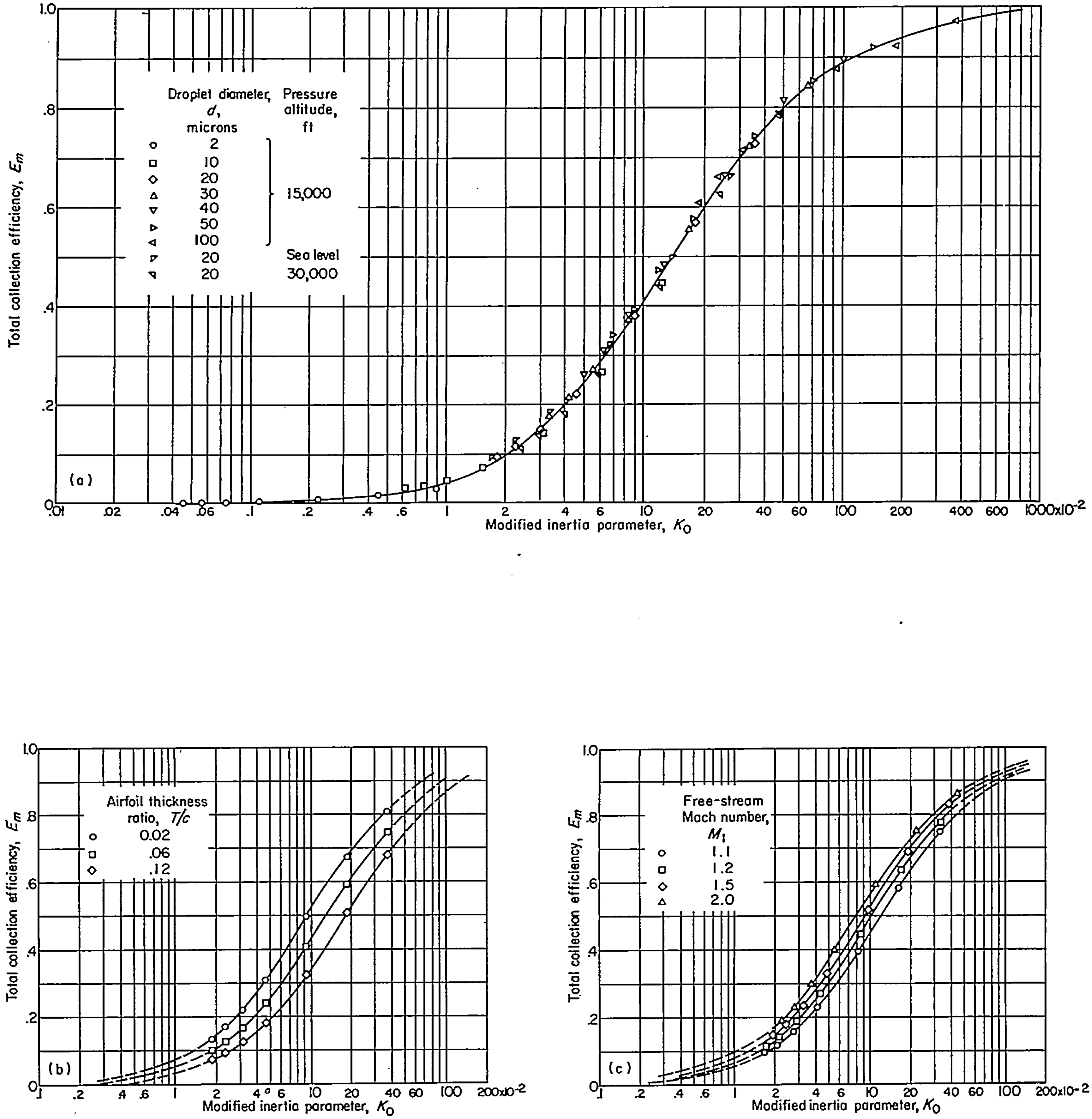

(a) Correlation of pressure altitude and droplet size. Free-stream Mach number, 1.3; airfoil thickness ratio, 0.06.
(b) Effect of thickness ratio. Droplet diameter, 20 microns; free-stream Mach number, 1.4; pressure altitude, 15,000 feet.
(c) Effect of free-stream Mach number. Droplet diameter, 20 microns; airfoil thickness ratio, 0.02; pressure altitude, 15,000 feet.

FIGURE 11.—Total collection efficiency of symmetrical double-wedge airfoils as function of modified inertia parameter. Free-stream static temperature, 440° R; angle of attack, 0°.

as for the NACA 0006-64 airfoil. Varying the chord length from 1 to 20 feet produces a change in the value of K_0 from 0.386 to 0.0193 for the double-wedge airfoil and from 0.266 to 0.0130 for the NACA 0006-64 airfoil. This variation in K_0 for both airfoils results in values of E_m of the same order of magnitude. For the given icing conditions, the following table lists for chord lengths of 4 and 20 feet the various pertinent parameters and variables, including the rate of total water catch on the airfoil per unit span for both airfoils:

Chord length, c, ft	Free-stream droplet Reynolds number, Re_1 (a)	Inertia parameter, K	Distance ratio, λ/λ_s (b)	Modified inertia parameter, K_0 (b)	Total collection efficiency, E_m	Rate of water catch, W, lb/(hr) (unit span)
Symmetrical double-wedge airfoil at M_1=1.5 (V_1=1051 mph)						
4	485	0.542	0.178	0.0965	0.432	17.9
20	485	.108	.178	.0193	.111	23.0
NACA 0006-64 airfoil at M_1=0.75 (V_1=526 mph)						
4	243	0.271	0.246	0.0665	0.330	6.85
20	243	.0542	.246	.0130	.128	13.3

[a] Values of viscosity of air obtained from linear variation with temperature given in ref. 16.
[b] Calculated as indicated in appendix D.

The rate of total water catch on the airfoil per unit span is calculated from

$$W_m = 0.3296 E_m T V_1 w$$

where T is in feet, w in grams per cubic meter, and V_1 in miles per hour. For this particular example, the table shows that for the 4-foot chord, the double-wedge airfoil has a somewhat larger value of E_m than the NACA 0006-64 airfoil; and for the 20-foot chord, the opposite is the case. Comparison of the two airfoils for a given chord length shows that, as expected, the effect of the total collection efficiency on the rate of water catch is small when compared with the free-stream velocity ratio chosen (2:1). The most significant comparison to be obtained from the table is that, for the double-wedge airfoil, increasing the chord length by a factor of 5 (from 4 to 20 ft) results in an increase of only 28 percent in the rate of water catch; whereas, for the NACA airfoil, a like change in the chord length results in an increase of 94 percent. This difference is the result of the fact that, unlike the local impingement on the rounded-leading-edge airfoils at free-stream Mach numbers less than critical, the local impingement at a given point on the surface of a double-wedge airfoil does not vary with the chord length of the airfoil, which is at a supersonic Mach number above the shock-wave-attachment Mach number.

APPENDIX D

TOTAL COLLECTION EFFICIENCY OF SYMMETRICAL DOUBLE-WEDGE AIRFOILS AS FUNCTION OF MODIFIED INERTIA PARAMETER

The total collection efficiency E_m is presented in figure 11 as a function of the modified inertia parameter K_0, as suggested in reference 14. The relation for K_0 is

$$K_0 = \frac{\lambda}{\lambda_s} K \tag{25}$$

where K is the inertia parameter, defined as

$$K = \frac{2}{9} \frac{\rho_w a^2 V_1}{\mu_1 c} \tag{24}$$

Since K is equal to λ_s/c (ref. 4), K_0 may also be written as

$$K_0 = \frac{\lambda}{\lambda_s} K = \frac{\lambda}{c}$$

The free-stream droplet Reynolds numbers used herein in calculating K_0 range up to 2104. The empirical drag law (eq. (5)) used in this report for the droplet motion in the moving reference frame is valid up to the Reynolds number of approximately 500. Therefore, for the values of K_0 presented in figure 11 (and also fig. 10), the values of λ/λ_s were obtained from table I of reference 4.

The curves of E_m against K_0 in figure 11 have exactly the same form as the curves of E_m against F_0, except that the use of K_0 results in a displacement of the entire curve toward larger abscissa values. The displacement of the E_m against K_0 curves obtained by varying the thickness ratio (fig. 11 (b)) or the free-stream Mach number (fig. 11 (c)) is less than the displacement of the E_m against F_0 curves obtained by the same procedures (figs. 9 (b) and (c)).

REFERENCES

1. Callaghan, Edmund E., and Serafini, John S.: Analytical Investigation of Icing Limit for Diamond Airfoil in Transonic and Supersonic Flow. NACA TN 2861, 1953.
2. Glauert, Muriel: A Method of Constructing the Paths of Raindrops of Different Diameters Moving in the Neighborhood of (1) a Circular Cylinder, (2) an Aerofoil, Placed in a Uniform Stream of Air; and a Determination of the Rate of Deposit of the Drops on the Surface and the Percentage of Drops Caught. R. & M. No. 2025, British A. R. C., 1940.
3. Kantrowitz, Arthur: Aerodynamic Heating and the Deflection of Drops by an Obstacle in an Air Stream in Relation to Aircraft Icing. NACA TN 779, 1940.
4. Langmuir, Irving, and Blodgett, Katherine B.: A Mathematical Investigation of Water Droplet Trajectories. Tech. Rep. No. 5418, Air Materiel Command, AAF, Feb. 19, 1946. (Contract No. W–33–038–ac–9151 with General Electric Co.)
5. Brun, Rinaldo J., and Mergler, Harry W.: Impingement of Water Droplets on a Cylinder in an Incompressible Flow Field and Evaluation of Rotating Multicylinder Method for Measurement of Droplet-Size Distribution, Volume-Median Droplet Size, and Liquid-Water Content in Clouds. NACA TN 2904, 1953.
6. Bergrun, Norman R.: A Method for Numerically Calculating the Area and Distribution of Water Impingement on the Leading Edge of an Airfoil in a Cloud. NACA TN 1397, 1947.
7. Guibert, A. G., Janssen, E., and Robbins, W. M.: Determination of Rate, Area, and Distribution of Impingement of Waterdrops on Various Airfoils from Trajectories Obtained on the Differential Analyzer. NACA RM 9A05, 1949.
8. Brun, Rinaldo J., Serafini, John S., and Moshos, George J.: Impingement of Water Droplets on an NACA 65_1–212 Airfoil at an Angle of Attack of 4°. NACA RM E52B12, 1952.
9. Lenherr, F. E., and Thomson, J. E.: Preliminary Report on the Computation of Water Drop Trajectories about a 6-Percent Airfoil. TDM–67, Northrop Aircraft, Inc., Aug. 14, 1952.
10. Brun, Rinaldo J., Serafini, John S., and Gallagher, Helen M.: Impingement of Cloud Droplets on Aerodynamic Bodies as Affected by Compressibility of Air Flow Around the Body. NACA TN 2903, 1953.
11. Tribus, Myron, and Guibert, Armand: Impingement of Spherical Water Droplets on a Wedge at Supersonic Speeds in Air. Jour. Aero. Sci., vol. 19, no. 6, June 1952, pp. 301–394.
12. Williams, Glenn Carber: Heat Transfer, Mass Transfer and Friction for Spheres. Sc. D. Thesis, M. I. T., 1942.
13. The Staff of the Ames 1- by 3-Foot Supersonic Wind-Tunnel Section: Notes and Tables for Use in the Analysis of Supersonic Flow. NACA TN 1428, 1947.
14. Sherman, P., Klein, J. S., and Tribus, M.: Determination of Drop Trajectories by Means of an Extension of Stokes' Law. Eng. Res. Inst., Air Res. and Dev. Command, USAF, Univ. Mich., Apr. 1952. (Contract AF 18 (600)–51, Proj. M992–D.)
15. Peirce, B. O.: A Short Table of Integrals. Third ed., Ginn and Co., 1929.
16. Diehl, Walter Stuart: Engineering Aerodynamics. Second ed., The Ronald Press Co., 1936.